

# Regularizing the Pulsar Timing Array likelihood: A path towards Fourier Space

Serena Valtolina<sup>ID\*</sup> and Rutger van Haasteren<sup>ID†</sup>

*Max Planck Institute for Gravitational Physics (Albert Einstein Institute),  
Leibniz Universität Hannover, Callinstrasse 38, D-30167, Hannover, Germany*

(Dated: December 17, 2024)

The recent announcement of evidence for a stochastic background of gravitational waves (GWB) in pulsar timing array (PTA) data has piqued interest across the scientific community. A combined analysis of all currently available data holds the promise of confirming the announced evidence as a solid detection of a GWB. However, the complexity of individual pulsar noise models and the variety of modeling tools used for different types of pulsars present significant challenges for a truly unified analysis. In this work we propose a novel approach to the analysis of PTA data: first a posterior distribution over Fourier modes is produced for each pulsar individually. Then, in a global analysis of all pulsars these posterior distributions can be re-used for a GWB search, which retains all information regarding the signals of interest without the added complexity of the underlying noise models or implementation differences. This approach facilitates combining radio and gamma-ray pulsar data, while reducing the complexity of the model and of its implementations when carrying out a GWB search with PTA data.

## I. INTRODUCTION

Pulsar Timing Array (PTA) experiments aim to detect a gravitational wave background (GWB) signal at nano-Hertz frequencies. Pulsars are extremely stable, rapidly rotating neutron stars characterized by narrow beams of radio emission. As the pulsar rotates, this collimated emission is detected by a radio telescope as a pulse-like signal. From stacking pulsar observations, we can obtain very high signal-to-noise ratio pulse templates and accurately predict the time of arrival (TOA) of each pulse (timing model, [1]). The differences between the observed TOAs and the TOAs predicted by the timing model are called timing residuals and can be explained as a combination of different effects, like, for example, instrumental noise, pulsar low-frequency noise due to rotational irregularities, and gravitational wave (GW) induced delays. The dominant GW signal that we expect to observe in the PTA frequency band ( $10^{-9}$ – $10^{-7}$  Hz) is a stochastic gravitational wave background (GWB). This signal affects the TOAs as a low-frequency noise common to all pulsars. Because of the quadrupolar nature of the GWB, the GW-induced residuals are spatially correlated among pulsars according to a specific correlation pattern called the Hellings and Downs (HD) function [2]. The HD correlation for a pair of pulsars depends only on the angular separation between them (as viewed from Earth) and predicts a positive correlation when the lines of sight to the pulsars are aligned (and anti-aligned), and negative correlations when the two lines of sight are almost orthogonal. This is a direct consequence of general relativity

and the quadrupolar description of GWs. Detecting the HD correlation is extremely important in a GWB search with PTAs, because this spatial correlation is the feature that allows us to distinguish between GW signal and the various noise processes that contribute to the pulsar timing data.

In the past couple of years, the PTA collaborations (the Chinese PTA (CPTA), the European PTA (EPTA) together with the Indian PTA (InPTA), the NANOGrav, the Parkes PTA (PPTA) and the MeerKAT PTA collaborations) have all released their new (radio) datasets and reported evidence for a common red process in their data that shows correlation properties between residuals of different pulsars, consistent with the sought HD correlation [3–7]. A larger number of pulsars and a longer observation time span will increase the sensitivity of the PTA experiments, which we expect to reach the detection threshold within the next few years [8, 9].

The main hypothesis for the source of this GWB signal is the incoherent superposition of continuous GW emission from a population of super-massive black hole binaries [10–14]. Nonetheless, a nano-Hertz frequency signal could be due to GWs generated by early Universe phenomena, such as cosmic strings interactions [e.g. 15, 16], curvature perturbations [e.g. 17, 18], quantum chromodynamics (QCD) phase transitions [e.g. 19, 20], non-standard inflationary scenarios [e.g. 21–23], and more. Those scenarios are comprehensively investigated in the new physics in the early Universe studies of the EPTA+InPTA and NANOGrav collaborations [24, 25].

In 2022, the Fermi-LAT collaboration also published the results of the first PTA analysis on gamma-ray pulsars [26]. Pulsar observations in the gamma band are very different from those at radio frequencies. During a typical pulsar observation with a radio-telescope, the continuous observations of the many pulses are carefully

\* serena.valtolina@aei.mpg.de

† rutger@vhaasteren.com

stacked together by averaging over the pulsar spin period (*folding* procedure, [1]). Comparing the obtained pulse profile with the highly precise telescope clock, we obtain a pulse’s TOA. For observations with Fermi-LAT, instead, modeling the results of the folding procedure to obtain the TOAs is more challenging. The Fermi-LAT collects individual gamma rays, for which arrival time and energy are registered. Furthermore, these observations are assigned a weight that estimates the probability that the photon was emitted by the pulsar pulse, or by unrelated fore/background sources [27–29]. Because of this uncertainty about the origin of the photons and the very low observed flux, reconstructing the pulsar’s pulse may require the folding of an observation with a very long duration. An alternative approach to folding for the evaluation of the TOAs has been presented in [30] (*photon-to-photon* approach). The latest update on the second Gamma-ray PTA data release status can be found at [31].

While the basic processing of TOAs and photons for both gamma-ray pulsars and radio pulsars can be done with `PINT` and `tempo2`—software packages for pulsar timing [32–35]—the search for gravitational waves requires more specific modeling techniques that are usually carried out using specialized software implementations. Historically, the fundamental differences between the radio data and the gamma-ray data have caused implementations of GW search to be highly specialized: packages like `enterprise` [36] or `forty-two` [37] can only process radio timing data, whereas the method of [30] is only able to analyze gamma-ray timing data. Modifying these packages for a combined radio and gamma-ray dataset is highly non-trivial, and requires significant development work. Our work makes this joint analysis easier.

When modeling a GWB signal in PTA data, the best estimate of the involved parameters is usually carried out through Bayesian inference: the posterior probability for each parameter is described as the product between a prior and a likelihood function. The likelihood function used for inference on radio PTA data [time-domain likelihood, 38–41] is very general and flexible, allowing the inclusion of many different signals in the model, including timing residual correlations. For gamma-ray data, instead, applications of the photon-to-photon approach have only produced upper limits on the amplitude of a possible GWB signal [31]. This approach only constrains common noise processes and does not use correlation information. In our paper, we present a regularization of the likelihood function that moves the analysis to the Fourier domain and allows the inclusion of correlated signals in the model (see Appendix A for a detailed discussion on the meaning of "regularization"). Most importantly, this method can be applied to both gamma-ray and radio data, independently of the package used to interpret the timing data

and build the signal model.

The other big advantage of using the method introduced in this paper is that it allows us to divide the GWB search into a two-step analysis. The first step focuses on individual pulsars and investigates those signals that are not covariant with a GWB (signals that are not describable as low-frequency (red) noises, such as deterministic signals and white noise). The second step, instead, analyses the full array of pulsars and focuses on the red noises, including the GWB. All signals investigated in the first step are marginalized over.

This paper shows the analytical derivation of a regularized formulation for the PTA likelihood in the Fourier domain, and presents some results from inference on real data. In detail, in Sec. II, we present a quick review of the time-domain likelihood definition (Sec. II B) and then derive in detail the regularized formulation in the Fourier domain (Sec. II C). Section III presents results for Bayesian inference runs on the EPTA DR2new dataset [42]. In particular, we show the comparison between posteriors obtained with the two likelihood formulations for the case of a single pulsar noise analysis (SPNA) on J1738+0333 (Sec. III A), and the results of a GWB search on the whole pulsars array (Sec. III B). We also briefly discuss applying this algorithm to the Gamma-ray PTA dataset in Sec. III C. We conclude by discussing advantages and future directions in Sec. IV.

## II. METHODS: TIME VS FOURIER DOMAIN

The primary data of a PTA analysis consists of the set of TOAs for an array of pulsars. The TOAs can be rewritten as the sum of a deterministic part  $f(t)$ , which is well-modeled by the timing model (which relativistic and propagation effects together with spin, spin-down, binary orbit modeling, etc.), and stochastic delays for which the delays are not modeled as a waveform but as a random process for which we only parameterize the distribution. The timing model definition and the evaluation of the expected TOAs at the Solar system barycenter is done using pulsar timing software packages like `tempo2` [34, 35] and `PINT` [32, 33]. The stochastic delays modeling includes signals such as measurement errors, pulsar low-frequency noise induced by rotational instabilities, dispersion due to the interstellar medium, and GW signals. In general, the observed times of arrival can be written as:

$$\begin{aligned} T^{obs} &= f(t; \boldsymbol{\beta}) + \delta \mathbf{t} \\ &= f(t; \boldsymbol{\beta}) + \delta \mathbf{t}_{WN} + \delta \mathbf{t}_{RN} + \delta \mathbf{t}_{DM} \\ &\quad + \delta \mathbf{t}_{GW} + \dots \end{aligned} \quad (1)$$

where  $\delta\mathbf{t} \equiv \sum_j \delta\mathbf{t}_{(j)}$  are the stochastic signal contributions and  $f(t; \boldsymbol{\beta})$  are the TOAs predicted by the timing model for the model parameters  $\boldsymbol{\beta}$ . The term  $\delta\mathbf{t}_{\text{WN}}$  refers to measurements errors (white noise),  $\delta\mathbf{t}_{\text{RN}}$  to pulsar spin noise, frequency-dependent delays due to interaction of the pulses with the interstellar medium (DM variations) are modeled by  $\delta\mathbf{t}_{\text{DM}}$ , and  $\delta\mathbf{t}_{\text{GW}}$  refers to the GW-induced delays. In Sec. II A, we show how each term of Eq. 1 is modeled.

In PTA data analysis, Bayesian inference is one of the most common strategies for obtaining information about model parameters. Given a data set  $D$ , the posterior probability distribution  $p(\Theta|D)$  for each parameter  $\Theta$  of the model is proportional to the product between a likelihood  $p(D|\Theta)$  and a prior function  $p(\Theta)$ . The likelihood function is defined as the probability density function of the data conditioned on the model and the model parameters. In Sec. II B, we present a brief overview of the PTA likelihood as it is coded in `enterprise` and used for inference on real data from PTA collaborations. The main references for this Section are [36, 38–41]. In Sec. II C, instead, we present our alternative formulation of the PTA likelihood in Fourier domain.

In the method we introduce in this paper, we carry out the analysis of an array of pulsars in multiple steps. First we analyze each pulsar individually in order to create a posterior distribution in Fourier space that can be analytically approximated. Then, in a second step, this analytical posterior distribution is used to form a global posterior distribution for the whole array of pulsars. All signals investigated in the first step can, with this method, be marginalized over. (Note that white noise parameters are usually kept fixed in GWB inference runs in an effort to limit the number of free parameters as much as possible for computational efficiency. With this method, those parameters can be marginalized over.)

Furthermore, moving to the Fourier domain makes the analysis more suitable for the inclusion of gamma-ray timing data alongside the radio ones without waiving the radio noise models' complexity and pulsar-specificity.

### A. TOAs: signal model components

The timing residuals  $\delta\mathbf{t}$  are obtained from the observed  $T^{\text{obs}}$  as  $\delta\mathbf{t} = T^{\text{obs}} - f(t; \boldsymbol{\beta})$  (Eq. 1). The term  $f(t)$  corresponds to the TOAs predicted by the timing model evaluated at the best-fit values  $\boldsymbol{\beta}_0$  (obtained from the timing analysis) for the timing parameters  $\boldsymbol{\beta}$ . From Eq. 1, we see that  $\delta\mathbf{t}$  can be rewritten as a sum of stochastic delay components. The main elements of this sum are listed in Eq. 1. We now describe in detail the model for each of those components.

The timing model ephemeris offsets  $\delta\mathbf{t}_{\text{TM}}$  are defined as the first-order linearization around the best-fit parameters (obtained from a previous analysis):

$$f(t; \boldsymbol{\beta}) = f(t; \boldsymbol{\beta}_0) + \delta\mathbf{t}_{\text{TM}} = f(t; \boldsymbol{\beta}_0) + M\xi. \quad (2)$$

The matrix  $M$  is called the design matrix and, given a timing model  $f(t; \boldsymbol{\beta})$ , it is defined as the matrix of the partial derivatives of the timing residuals with respect to the timing model parameters:  $M_{jk} \equiv (\partial f(t_j; \boldsymbol{\beta}) / \partial \beta_k) |_{\boldsymbol{\beta}_0}$ . The vector  $\xi$  represents the ephemeris offsets:  $\xi \equiv \boldsymbol{\beta} - \boldsymbol{\beta}_0$ .

The white noise component  $\delta\mathbf{t}_{\text{WN}}$  depends upon the measurement uncertainty of the TOAs:  $\sigma_{\text{TOA}}$ . The covariance of those noise components is usually modeled as a function of two sets of parameters (EFAC ( $\mathcal{E}$ ) and EQUAD ( $\mathcal{Q}$ )) specific for each observing system (particular configuration of observing backend and receiver):

$$\langle \delta\mathbf{t}_{\text{WN}, \mu i} \delta\mathbf{t}_{\text{WN}, \nu j} \rangle_{\text{pr}} = \mathcal{E}_\mu^2 \sigma_{\text{TOA}, i}^2 \delta_{ij} \delta_{\mu\nu} + \mathcal{Q}_\mu^2 \delta_{ij} \delta_{\mu\nu}, \quad (3)$$

where the indices  $i$  and  $j$  label the observation, and  $\mu, \nu$  label the observing system.<sup>1</sup> An additional white noise component describing the pulse phase jitter (commonly known as jitter noise or ECORR( $\mathcal{J}$ )) can also be included. This additional noise parameter models correlated white noise between TOAs observed at the same epoch at different radio frequencies. It can be added to Eq. 3 as an additional EQUAD parameter:  $\mathcal{J}_\mu^2 \delta_{\mu\nu} \delta_{ef}$ , where  $e$  and  $f$  label the observed epochs.

The chromatic ( $\delta\mathbf{t}_{\text{DM}}$ ) and achromatic ( $\delta\mathbf{t}_{\text{RN}}$  and  $\delta\mathbf{t}_{\text{GW}}$ ) low frequency processes are modeled as Gaussian processes [41]. They are written as a discrete sum of cosine and sine functions evaluated at determined frequencies:

$$\delta\mathbf{t}_{\text{RN/DM}} = \sum_k \left[ a_k \cos(2\pi kt/T) + b_k \sin(2\pi kt/T) \right] \nu_{\text{obs}}^\alpha, \quad (4)$$

where  $T$  is the total time of observation, and  $\alpha = 0$  for RN and  $\alpha = -2$  for DM. In matrix notation:

$$\begin{aligned} \delta\mathbf{t}_{\text{RN}} + \delta\mathbf{t}_{\text{GW}} &= F\mathbf{a} \\ \delta\mathbf{t}_{\text{DM}} &= F_{\text{DM}}\mathbf{a}_{\text{DM}}, \end{aligned} \quad (5)$$

where  $\mathbf{a}$  and  $\mathbf{a}_{\text{DM}}$  are the Fourier coefficients of  $\delta\mathbf{t}_{\text{RN}}$  and  $\delta\mathbf{t}_{\text{DM}}$  respectively. The matrices  $F$  and  $F_{\text{DM}}$  (often referred to as Fourier design matrices) are the linear transformation corresponding to a discrete Fourier transform with the ‘‘backward’’ normalization [conventions as in `scipy` 43]. The Fourier design matrix for

<sup>1</sup> In this paper, we use  $\langle \cdot \rangle$  to indicate the covariance under the posterior distribution:  $\langle ab \rangle = \text{cov}(a, b)$ . When we evaluate the covariance under the prior distribution instead, we use the notation  $\langle \cdot \rangle_{\text{pr}}$ .

the chromatic noise has an additional factor that includes the dependence upon the observing radio frequency  $\nu_{obs}$ :  $F_{DM,ij} = F_{ij} \times (\nu_{obs}/1400\text{MHz})^{-2}$ .

The prior covariance matrix of the Fourier coefficients  $\phi_{\text{RN/DM}} = \langle \mathbf{a}_{\text{RN/DM}} \mathbf{a}_{\text{RN/DM}}^T \rangle_{\text{pr}}$  depends upon the hyperparameters  $\boldsymbol{\rho}$  of the corresponding noise process:

$$\begin{aligned} [\phi_{\text{RN}}]_{(a,b)(j,k)} &\equiv \Gamma_{ab} \delta_{jk} S_{\text{GWB}}(f_j; \boldsymbol{\rho}_{\text{GWB}}) \\ &\quad + \delta_{ab} \delta_{jk} S_{\text{RN}}(f_j; \boldsymbol{\rho}_{\text{RN}}) \\ [\phi_{\text{DM}}]_{(a,b)(j,k)} &\equiv \delta_{ab} \delta_{jk} S_{\text{DM}}(f_j; \boldsymbol{\rho}_{\text{DM}}), \end{aligned} \quad (6)$$

where  $a, b$  label the pulsar,  $j, k$  label the frequency components,  $\Gamma_{ab}$  is the Hellings Downs (HD) correlation, and  $S(f; \boldsymbol{\rho})$  is the power spectral density at frequency  $f$ , described by the hyperparameters  $\boldsymbol{\rho}$ . In absence of pulsar-correlated signals, the  $\phi$  matrix is diagonal.

The noise components just described are usually written with the following compact notation:

$$M\boldsymbol{\xi} + F\mathbf{a} + F_{\text{DM}}\mathbf{a}_{\text{DM}} = T\mathbf{b}. \quad (7)$$

See Table I for a complete summary of the notation used through this paper.

## B. The time-domain PTA likelihood

In this Section, we present a brief overview of the PTA likelihood as it is coded in `enterprise` and used for inference on real data from PTA collaborations. The main references for this Section are [36, 38–41].

When inferring the noise properties of a single pulsar, the posterior distribution for the model parameters  $(\mathbf{b}, \boldsymbol{\rho}, \boldsymbol{\theta})$  (product of likelihood function and prior distribution) is usually written as:

$$\begin{aligned} p(\mathbf{b}, \boldsymbol{\rho}, \boldsymbol{\theta} | \delta\mathbf{t}) p(\delta\mathbf{t}) &= p(\delta\mathbf{t} | \mathbf{b}, \boldsymbol{\theta}) p(\mathbf{b} | \boldsymbol{\rho}) p(\boldsymbol{\rho}) p(\boldsymbol{\theta}) \\ p(\delta\mathbf{t} | \mathbf{b}, \boldsymbol{\theta}) &= \frac{\exp\left[-\frac{1}{2}(\delta\mathbf{t} - T\mathbf{b})^T N^{-1}(\delta\mathbf{t} - T\mathbf{b})\right]}{\sqrt{\det(2\pi N)}} \\ p(\mathbf{b} | \boldsymbol{\rho}) &= \frac{\exp\left[-\frac{1}{2}\mathbf{b}^T B^{-1}\mathbf{b}\right]}{\sqrt{\det(2\pi B)}}, \end{aligned} \quad (8)$$

where  $N \equiv \langle \delta\mathbf{t}_{\text{WN}} \delta\mathbf{t}_{\text{WN}}^T \rangle_{\text{pr}}$ , and  $T$  and  $\mathbf{b}$  are defined in Eq. 7. The quantity  $P(\delta\mathbf{t})$  is the evidence or fully marginalized likelihood, often denoted as  $Z$ . Going forward, we omit the  $P(\delta\mathbf{t})$  occasionally and instead use a  $\propto$  for readability.  $\boldsymbol{\theta}$  represents the white noise parameters. The second exponential on the rhs describes the conditioned probability of  $\mathbf{b}$  upon the model hyperparameters  $\boldsymbol{\rho}$ . The prior matrix  $B$  is a block-diagonal matrix defined as

$$B \equiv \begin{bmatrix} \infty & 0 & 0 \\ 0 & \phi_{\text{RN}} & 0 \\ 0 & 0 & \phi_{\text{DM}} \end{bmatrix} = \begin{bmatrix} \infty & 0 \\ 0 & \phi \end{bmatrix} \quad (9)$$

where we assigned an improper infinite prior to the timing model ephemeris offsets  $\boldsymbol{\xi}$ . Using improper priors on  $\boldsymbol{\xi}$  is customary in pulsar timing. Although adding more realistic Gaussian priors on  $\boldsymbol{\xi}$  is trivial, the data is so informative with respect to the prior that there is no practical need to change the practice of using improper priors.

The posterior distribution in Eq. 8 can be generalized to the case of an array of pulsars:

$$\begin{aligned} p(\{\mathbf{b}\}, \boldsymbol{\rho}, \boldsymbol{\theta} | \{\delta\mathbf{t}\}) &= \\ &\left[ \prod_{j=1}^{N_p} \frac{p(\delta\mathbf{t}_j | \mathbf{b}_j, \boldsymbol{\theta})}{p(\delta\mathbf{t}_j)} \right] p(\{\mathbf{b}\} | \boldsymbol{\rho}) p(\boldsymbol{\rho}) p(\boldsymbol{\theta}), \end{aligned} \quad (10)$$

where  $N_p$  is the number of pulsars.

Carrying out a Bayesian inference run with the full likelihood in Eq. 10 would be challenging to sample because of the very high number of parameters, combined with the challenging parameter covariances [44]. Usually, the analysis aims to obtain estimates of the noise hyperparameters  $\boldsymbol{\rho}$ . To do that, we use the marginalized posterior distribution over the timing model parameters and Fourier coefficients. Integrating Eq. 10 over  $d^{N_p}\mathbf{b}$  we obtain:

$$\begin{aligned} p(\boldsymbol{\rho}, \boldsymbol{\theta} | \{\delta\mathbf{t}\}) &\propto \int d^{N_p}\mathbf{b} \left[ \prod_{j=1}^{N_p} p(\delta\mathbf{t}_j | \mathbf{b}_j, \boldsymbol{\theta}) \right] p(\{\mathbf{b}\} | \boldsymbol{\rho}) p(\boldsymbol{\rho}) p(\boldsymbol{\theta}) \\ &= \frac{\exp\left[-\frac{1}{2}\delta\mathbf{t}^T C^{-1}\delta\mathbf{t}\right]}{\sqrt{\det(2\pi C)}} p(\boldsymbol{\rho}) p(\boldsymbol{\theta}), \end{aligned} \quad (11)$$

where  $C \equiv N + TBT^T$ . See [38, 41] for more detailed descriptions of the PTA likelihood marginalization.

## C. The regularized PTA likelihood

This work introduces a regularization of the PTA likelihood function that allows us to move the analysis to the Fourier space and reduces the complexity of a GWB search over the pulsars array. When moving to the Fourier domain, the regularization term is the key element to prevent overfitting the PTA data (see Appendix A for more details about overfitting issues when moving to a representation in Fourier domain).

This regularization of the PTA likelihood is useful because (i) it makes straightforward to combine radio timing residuals and gamma-ray data, and (ii) it allows us to divide a GWB inference on a PTA dataset in a two-step analysis. These two steps can be briefly described as follows:

**Step 1:** inference on the parameters of all the signal processes that are not covariant with a GWB.

Symbol	Description
$\boldsymbol{\beta}$	timing model parameters ( $\boldsymbol{\beta}_0$ are the best-fit values)
$T^{obs}$	observed TOAs
$f(t; \boldsymbol{\beta})$	timing model predicted TOAs for the model parameters $\boldsymbol{\beta}$
$\delta \mathbf{t}$	timing residuals $\delta \mathbf{t} \equiv T^{obs} - f(t; \boldsymbol{\beta}_0)$
$M$	design matrix $M_{jk} \equiv (\partial f(t_j; \boldsymbol{\beta}) / \partial \beta_k)  _{\boldsymbol{\beta}_0}$
$\boldsymbol{\xi}$	ephemeris offsets $\boldsymbol{\xi} \equiv \boldsymbol{\beta} - \boldsymbol{\beta}_0$
$\sigma_{TOA}$	measurement error associated to the TOA
$F$	Fourier design matrix
$\mathbf{a}$	Fourier coefficients
$T$	$T \equiv [M, F]$
$\mathbf{b}$	$\mathbf{b} \equiv \begin{bmatrix} \boldsymbol{\xi} \\ \mathbf{a} \end{bmatrix}$
$\boldsymbol{\theta}$	deterministic signals and white noise parameters
$\boldsymbol{\rho}$	noise hyperparameters
$\phi$	$\phi_{RN/DM} \equiv \langle \mathbf{a}_{RN/DM} \mathbf{a}_{RN/DM}^T \rangle_{pr}$ (Eq. 6)
$B$	prior matrix $B \equiv \text{diag}(\infty, \phi_{RN}, \phi_{DM})$ , $B^{-1} = \text{diag}(0, (\phi_{RN})^{-1}, (\phi_{DM})^{-1})$
$N$	white noise covariance matrix $N \equiv \langle \delta \mathbf{t}_{WN} \delta \mathbf{t}_{WN}^T \rangle_{pr}$
$N_p$	number of pulsars
$C$	covariance matrix of the fully marginalized likelihood: $C \equiv N + TBT^T$
$\tilde{N}$	$\tilde{N}^{-1} \equiv N^{-1} - N^{-1}M(M^T N^{-1}M)^{-1}M^T N^{-1}$ .
$\Sigma$	$\Sigma^{-1} \equiv F^T \tilde{N}^{-1} F + \phi^{-1}$
$\hat{\mathbf{a}}$	optimal estimator of the Fourier coefficients $\hat{\mathbf{a}} \equiv \Sigma F^T \tilde{N}^{-1} \delta \mathbf{t}$

Table I. Notation summary.

Those are white noise and deterministic signals like, for example, DM dips. In this step, each pulsar is analyzed *individually*. The noise signals covariant with a GWB (RN, DM variations, etc.) are still included in the model, but their hyperparameters are fixed.

**Step 2:** inference on the hyperparameters of the GWB and all signals covariant with it (RN, DM variations, etc.). Here, the analysis runs over the *whole array* of pulsars. The parameters investigated in *Step 1* are marginalized over.

The main idea behind the derivation of the regularized likelihood formulation from the time-domain one can be visualized starting from the general definition of the PTA joint hierarchical likelihood function:

$$p(\delta \mathbf{t} | \boldsymbol{\theta}, \mathbf{a}_{RN}, \mathbf{a}_{DM}) p(\mathbf{a}_{RN} | \boldsymbol{\rho}_{RN}) p(\mathbf{a}_{DM} | \boldsymbol{\rho}_{DM}). \quad (12)$$

Here,  $\delta \mathbf{t}$  are the timing residuals,  $\boldsymbol{\theta}$  are the parameters used to describe white noise and other deterministic signals,  $\mathbf{a}$  and  $\boldsymbol{\rho}$  are, respectively, the Fourier coefficients and the hyperparameters that describe the RN and DM variations for each pulsar. A complete summary of the notation used in this paper can be found in Table I.

The posterior probability density for a single pulsar can be written (according to the Bayes theorem) as the product of likelihood and prior probability distributions:

$$p(\boldsymbol{\theta}, \mathbf{a}_{RN}, \boldsymbol{\rho}_{RN}, \mathbf{a}_{DM}, \boldsymbol{\rho}_{DM} | \delta \mathbf{t}) = p(\delta \mathbf{t} | \boldsymbol{\theta}, \mathbf{a}_{RN}, \mathbf{a}_{DM}) p(\mathbf{a}_{RN} | \boldsymbol{\rho}_{RN}) p(\mathbf{a}_{DM} | \boldsymbol{\rho}_{DM}) \times p(\boldsymbol{\rho}_{RN}) p(\boldsymbol{\rho}_{DM}) p(\boldsymbol{\theta}) / p(\delta \mathbf{t}). \quad (13)$$

For any fixed set of noise hyperparameters  $[\boldsymbol{\rho}_{RN_0}, \boldsymbol{\rho}_{DM_0}]$  and parameters  $\boldsymbol{\theta}$ ,  $p(\mathbf{a}_{RN}, \boldsymbol{\rho}_{RN_0}, \mathbf{a}_{DM}, \boldsymbol{\rho}_{DM_0} | \boldsymbol{\theta}, \delta \mathbf{t})$  can be rewritten as a Gaussian distribution in Fourier domain. Thus, Eq. 13 can be rewritten as the product of Gaussian probability distributions as a function of the Fourier coefficients:

$$p(\mathbf{a}_{RN}, \boldsymbol{\rho}_{RN}, \mathbf{a}_{DM}, \boldsymbol{\rho}_{DM} | \boldsymbol{\theta}, \delta \mathbf{t}) = p(\mathbf{a}_{RN}, \mathbf{a}_{DM} | \boldsymbol{\theta}, \boldsymbol{\rho}_{RN_0}, \boldsymbol{\rho}_{DM_0}) \times \frac{p(\mathbf{a}_{RN} | \boldsymbol{\rho}_{RN}) p(\mathbf{a}_{DM} | \boldsymbol{\rho}_{DM}) p(\boldsymbol{\rho}_{RN}) p(\boldsymbol{\rho}_{DM})}{p(\mathbf{a}_{RN} | \boldsymbol{\rho}_{RN_0}) p(\mathbf{a}_{DM} | \boldsymbol{\rho}_{DM_0}) p(\boldsymbol{\rho}_{RN_0}) p(\boldsymbol{\rho}_{DM_0})}, \quad (14)$$

where the final ratio of prior distributions acts as a “reweighting term”.

The  $\boldsymbol{\theta}$  parameters describe all the signal models that are not covariant with the Gaussian processes modeled

in the Fourier domain. Thus, when marginalizing over them, Eq. 13 is not an equivalence anymore, but it is still a good approximation. This is a general description of the method; we now describe the expressions for all the involved probability distributions in more detail.

The hierarchical formulation of the joint likelihood function for PTA (Eq. 12- 13) was first introduced in [38]. It was then expanded in [41] to optimize the modeling of pulsar noise processes as Gaussian processes. In [44] the authors showed how the hierarchical formulation of the PTA likelihood could allow for Hamiltonian sampling in PTA data analysis. Recently, [45] used the same likelihood factorization to explore the capabilities of Gibbs sampling in SPNA and [46] ex-

panded those findings to derive the most general, agnostic, per-frequency Bayesian search for a low-frequency noise process in PTA data. An alternative likelihood factorization allowing the division of the GWB search in a two-step analysis was presented in [47] (factorized likelihood technique). This method models pulsars autocorrelation terms only; thus, it allows searches for the amplitude of a common process but does not investigate pulsars cross correlations. Our method, instead, is capable of searching pulsar correlated signals.

Let's derive the regularized formulation in Fourier domain of the PTA likelihood step by step. The starting point consists of marginalizing the full PTA likelihood in Eq. 10 over the timing ephemeris offsets:

$$\begin{aligned}
p(\{\mathbf{a}\}, \boldsymbol{\rho}, \boldsymbol{\theta} | \{\delta\mathbf{t}\}) &\propto \int d^{N_p} \boldsymbol{\xi} \left[ \prod_{j=1}^{N_p} p(\delta\mathbf{t}_j | \mathbf{b}_j) \right] p(\{\mathbf{b}\} | \boldsymbol{\rho}) p(\boldsymbol{\rho}) p(\boldsymbol{\theta}) \\
&= \frac{\exp\left[-\frac{1}{2}(\delta\mathbf{t} - F\mathbf{a})^T \tilde{N}^{-1}(\delta\mathbf{t} - F\mathbf{a})\right]}{\sqrt{\det(2\pi N)} \sqrt{\det(2\pi M^T N^{-1} M)}} \frac{\exp\left[-\frac{1}{2}\mathbf{a}^T \phi^{-1} \mathbf{a}\right]}{\sqrt{\det(2\pi\phi)}} p(\boldsymbol{\rho}) p(\boldsymbol{\theta}),
\end{aligned} \tag{15}$$

where  $\tilde{N}^{-1} \equiv N^{-1} - N^{-1}M(M^T N^{-1}M)^{-1}M^T N^{-1}$ . We also introduced  $\mathbf{a}$  which is the vector of all Fourier coefficients (dimension:  $(N_p \times (N_{a,\text{RN}} + N_{a,\text{DM}}), 1)$ ),  $\boldsymbol{\rho}$  is the vector of all RN and DM hyperparameters for each pulsar, and  $\phi$ , which represents the prior matrix without the timing model components (see Eq. 9). The white noise covariance matrix  $N$  depends on the model parameters  $\boldsymbol{\theta}$ . Note that Eq. 11 is marginalized over both timing model parameters and Fourier coefficients. Thus, the integral of Eq. 15 over the Fourier coefficients is equivalent to Eq. 11.

Introducing the definitions  $\Sigma^{-1} \equiv F^T \tilde{N}^{-1} F + \phi^{-1}$  and  $\hat{\mathbf{a}} \equiv \Sigma F^T \tilde{N}^{-1} \delta\mathbf{t}$ , Eq. 15 can be rewritten as:

$$\begin{aligned}
\ln p(\{\mathbf{a}\}, \boldsymbol{\rho}, \boldsymbol{\theta} | \{\delta\mathbf{t}\}) &= -\frac{1}{2}(\mathbf{a} - \hat{\mathbf{a}})^T \Sigma^{-1}(\mathbf{a} - \hat{\mathbf{a}}) - \frac{1}{2}\delta\mathbf{t}^T \tilde{N}^{-1} \delta\mathbf{t} + \frac{1}{2}\hat{\mathbf{a}}^T \Sigma^{-1} \hat{\mathbf{a}} \\
&\quad - \frac{1}{2} \left[ \ln \det(2\pi N) + \ln \det(2\pi M^T N^{-1} M) + \ln \det(2\pi\phi) \right] \\
&\quad + \ln p(\boldsymbol{\rho}) + \ln p(\boldsymbol{\theta}) + \text{const},
\end{aligned} \tag{16}$$

where only the first term depends upon the Fourier coefficients  $\mathbf{a}$ . For any fixed set of noise hyperparameters  $\boldsymbol{\rho}_0$ , we define  $\phi_0 \equiv \phi(\boldsymbol{\rho}_0)$ ,  $\Sigma_0 \equiv \Sigma(\boldsymbol{\rho}_0)$  and  $\hat{\mathbf{a}}_0 \equiv \hat{\mathbf{a}}(\boldsymbol{\rho}_0)$ . Thus, from Eq. 16 it is immediate to see that  $p(\{\mathbf{a}\}, \boldsymbol{\rho}_0, \boldsymbol{\theta} | \{\delta\mathbf{t}\})$  is a multivariate Gaussian in  $\mathbf{a}$ . Note that the phase information is contained in  $\hat{\mathbf{a}}_0 = \Sigma_0 F^T \tilde{N}^{-1} \delta\mathbf{t}$ ; the  $\hat{\mathbf{a}}_0$  effectively replace the data  $\delta\mathbf{t}$  of our original likelihood function.

Finally, we can write a general expression of the PTA posterior as the product of Eq. 16 with  $\boldsymbol{\rho} = \boldsymbol{\rho}_0$  and a reweighting term consisting in the ratio between prior distributions for free and fixed noise parameters  $\boldsymbol{\rho}$  (as shown in Eq. 14):

$$\begin{aligned}
\ln p(\{\mathbf{a}\}, \boldsymbol{\rho}, \boldsymbol{\theta} | \{\delta\mathbf{t}\}) &= \ln p(\{\mathbf{a}\}, \boldsymbol{\rho}_0, \boldsymbol{\theta} | \{\delta\mathbf{t}\}) + \ln p(\{\mathbf{a}\} | \boldsymbol{\rho}) + \ln p(\boldsymbol{\rho}) - \ln p(\{\mathbf{a}\} | \boldsymbol{\rho}_0) - \ln p(\boldsymbol{\rho}_0) + \ln p(\boldsymbol{\theta}) \\
&= \ln p(\{\mathbf{a}\}, \boldsymbol{\rho}_0, \boldsymbol{\theta} | \{\delta\mathbf{t}\}) - \frac{1}{2}\mathbf{a}^T \phi^{-1} \mathbf{a} - \frac{1}{2} \ln \det(2\pi\phi) + \frac{1}{2}\mathbf{a}^T \phi_0^{-1} \mathbf{a} + \frac{1}{2} \ln \det(2\pi\phi_0) + \ln p(\boldsymbol{\theta}).
\end{aligned} \tag{17}$$

Marginalizing Eq. 17 over the Fourier coefficients  $\mathbf{a}$ , we obtain the final expression for the posterior distribution

of the  $\boldsymbol{\rho}$  hyperparameters using the regularized full PTA likelihood in Fourier domain:

$$\begin{aligned} \ln p(\boldsymbol{\rho}, \boldsymbol{\theta} | \{\delta \mathbf{t}\}) &= \int d^{N_p} \mathbf{a} \ln \left[ p(\{\mathbf{a}\}, \boldsymbol{\rho}_0, \boldsymbol{\theta} | \{\delta \mathbf{t}\}) p(\boldsymbol{\theta}) \times \frac{p(\{\mathbf{a}\} | \boldsymbol{\rho}) p(\boldsymbol{\rho})}{p(\{\mathbf{a}\} | \boldsymbol{\rho}_0) p(\boldsymbol{\rho}_0)} \right] \\ &= \frac{1}{2} \hat{\mathbf{a}}_0^T \Sigma_0^{-1} \Sigma^{-1} \Sigma_0^{-1} \hat{\mathbf{a}}_0 - \frac{1}{2} \delta \mathbf{t}^T \tilde{N}^{-1} \delta \mathbf{t} + \ln p(\boldsymbol{\theta}) \\ &\quad - \frac{1}{2} [\text{Lndet}(2\pi N) + \text{Lndet}(2\pi M^T N^{-1} M) + \text{Lndet}(2\pi \phi) - \text{Lndet}(2\pi \Sigma)]. \end{aligned} \quad (18)$$

Note that  $\Sigma^{-1} = \Sigma_0 - \phi_0^{-1} + \phi^{-1}$ . If the  $\boldsymbol{\theta}$  parameters are fixed, Eq. 18 is analytically equivalent to Eq. 11.

One of the main advantages of this regularized formulation (Eq. 18) is that it allows dividing a GWB inference on a PTA dataset in a two-step analysis, where deterministic signals and white noise are investigated separately for each pulsar and marginalized over when moving to analyze the whole array. We now describe the details of these two steps.

### 1. Step 1:

In this step, each pulsar is analyzed *individually*. From the complete pulsar noise model, we infer the parameters of the signals that are not covariant with a GWB: inferred parameters of white noise and deterministic signals (like, for example, exponential dips (DM dips) which consist in sudden radio frequency-dependent advance of pulse arrival times probably due to a drop in the density of the ionized interstellar medium along the line of sight to the pulsar [48]) are expected to be approximately independent from the GWB model. We sample over these parameters  $\boldsymbol{\theta}$ , while the hyperparameters of the signals covariant with a GWB (RN, DM variations, and other chromatic – dependent on the observation frequency – and achromatic – independent of the observation frequency – low-frequency processes) are fixed. We are free to choose the hyperparameter values  $\boldsymbol{\rho}_0$ . See Appendix A for a discussion on the freedom and limitations of this choice. The likelihood function used in this step is the time-domain one.

### 2. Step 2:

We consider now the *whole array* of pulsars and run inference over the hyperparameters of the GWB and all signals covariant with it (RN, DM variations, ...) using the Fourier posterior distribution formula (Eq. 18). The parameters sampled in the previous step (white noise, etc.) have therefore been marginalized over. Before starting to sample, we need to build the quantities  $\Sigma_0$  and  $\hat{\mathbf{a}}_0$  for the whole array, which cor-

respond to the variance and mean of the distribution  $\mathcal{N}(\mathbf{a}_{\text{RN}}, \mathbf{a}_{\text{DM}} | \boldsymbol{\theta}, \boldsymbol{\rho}_{\text{RN}_0}, \boldsymbol{\rho}_{\text{DM}_0})$ .

We estimate  $\Sigma_0$  and  $\hat{\mathbf{a}}_0$  from the results obtained in *Step 1*. The analytical formulas are:

$$\begin{aligned} \Sigma_0^{-1} &= F^T \tilde{N}^{-1} F + \phi_0^{-1} \\ \hat{\mathbf{a}}_0 &= \Sigma_0 F^T \tilde{N}^{-1} \delta \mathbf{t}. \end{aligned} \quad (19)$$

Those depend on the parameters  $\boldsymbol{\theta}$  and the timing residuals  $\delta \mathbf{t}$ . For a chain sample  $\boldsymbol{\theta}_i$  of the white noise parameters (obtained in *Step 1*), we can evaluate  $\hat{\mathbf{a}}_{0i}$  and  $\Sigma_{0i}$ . Given a set of such samples, we can approximate the mean and variance of the normal distribution  $\mathcal{N}(\mathbf{a}_{\text{RN}}, \mathbf{a}_{\text{DM}} | \boldsymbol{\theta}, \boldsymbol{\rho}_{\text{RN}_0}, \boldsymbol{\rho}_{\text{DM}_0})$  as

$$\begin{aligned} \hat{\mathbf{a}}_0 &= \text{mean}(\hat{\mathbf{a}}_{0i}) \\ \Sigma_0 &= \frac{1}{N_s - 1} \left[ \sum_{i=1}^{N_s} (\Sigma_{0i} + \hat{\mathbf{a}}_{0i} \hat{\mathbf{a}}_{0i}^T) - N_s \hat{\mathbf{a}}_0 \hat{\mathbf{a}}_0^T \right], \end{aligned} \quad (20)$$

where  $N_s$  is the number of samples considered from the white noise chain. This method to approximate the mean  $\hat{\mathbf{a}}_0$  and variance  $\Sigma_0$  of the normal distribution would correspond to reconstructing the distribution from an infinite number of Fourier coefficients samples. See Appendix B for a complete derivation of Eq. 20.

We now have all the elements to use Eq. 18 to run inference over the whole pulsars array and obtain posterior distributions for the  $\boldsymbol{\rho}$  hyperparameters.

## III. APPLICATION AND EXAMPLES

In this section, we discuss the implementation of the method described in Sec. II C when carrying out Bayesian inference runs over a PTA dataset. We use the 25 pulsars of the EPTA DR2new dataset [42] and compare our results with the results obtained with the “standard” likelihood (Eq. 11) coded in `enterprise` [36]. We first discuss the example of a SPNA for the pulsar J1738+0333, and then show the results of a GWB search on the full pulsars array.

### A. Pulsar J1738+0333: an example of SPNA

The timing solution of the pulsar J1738+0333 is based on data collected with the Arecibo and the EPTA telescopes. For the analysis described in this work, we use the EPTA DR2new data [49]. The noise analysis carried out by the EPTA collaboration is described in [50]. Evaluating the Bayes factor between different noise models, they show that in the DR2new dataset a noise model with a chromatic noise-only is slightly favored with respect to one that contains both chromatic and achromatic noise contributions.

We present here the results for a SPNA carried out on J1738+0333 (EPTA DR2new data) with our regularized likelihood. We defined a noise model that includes EFAC and EQUAD (which model the TOAs measurements uncertainty, white noise) specific for each observing system, and RN and DM variations, both modeled as stationary Gaussian processes with a *flat-tail power-law spectrum*:

$$S_y(f; A_y, \gamma_y, k_y) = \max\left(\frac{A_y^2}{12\pi^2} \left(\frac{f}{yr^{-1}}\right)^{-\gamma_y} yr^3, k_y^2\right), \quad (21)$$

where the subscript “y” refers either to RN or DM variations. The reasoning behind using a flat-tail power-law instead of a simple power-law model is discussed in Appendix A. We model RN and DM over, respectively, 30 and 100 frequency bins.

We follow the methodology described in Sec. II C to obtain posterior distributions for the RN and DM variations hyperparameters. We used the Markov Chain Monte Carlo (MCMC) sampler PTMCMCSampler [51]. Firstly, we sampled over the white noise parameters using the time-domain likelihood (Eq. 11), while setting the RN and DM hyperparameters fixed to  $\log_{10}A = -12$ ,  $\gamma = 5$  and  $\log_{10}k = -5$  (*Step 1*). We used the results to estimate  $\Sigma_0$  and  $\hat{\mathbf{a}}_0$  as described in Eq. 20, and then run inference over the RN and DM hyperparameters using Eq. 18 (*Step 2*). A summary of the prior distributions considered for these analyzes can be found in Table II.

We show in Fig. 1 the posteriors obtained for the RN and DM variations hyperparameters with the regularized likelihood (orange curves). Those are compared with the posteriors obtained for a full SPNA using the traditional likelihood (Eq. 11, blue curve). The RN and DM posteriors obtained with our method (*Step 1* + *Step 2*) are equivalent to what one would obtain sampling over all the noise parameters (including the white noise ones we marginalize over in *Step 1*) with the time-domain likelihood. The slight widening of the orange posteriors, compared to the blue ones, is due to the fact that we are marginalizing over the white noise parameters. Even though white noise parameters and GWB hyperparameters are expected to be not covari-

	free parameter	prior type	interval
Step 1	EFAC ( $\mathcal{E}$ )	uniform	[0.5, 5]
	EQUAD ( $\mathcal{Q}$ )	log-uniform	[-10, -5]
	$\log_{10}A_{\text{DMdip}}$	log-uniform	[-10, -2]
	$\log_{10}\tau_{\text{DMdip}}$	log-uniform	[0, 2.5]
	$t_{0\text{DMdip}}$	uniform	$[t_{\min}, t_{\max}]$
Step 2	$\log_{10}A_{\text{RN/DM/chrom}}$	log-uniform	[-18, -12]
	$\gamma_{\text{RN/DM/chrom}}$	uniform	[0, 7]
	$\log_{10}k_{\text{RN/DM/chrom}}$	log-uniform	[-9, -4]
	$\log_{10}A_{\text{GWB}}$	log-uniform	[-15.5, -13.5]
	$\gamma_{\text{GWB}}$	uniform	[0, 7]

Table II. Prior distributions as defined for the samplings.

ant, marginalizing over the white noise parameters is statistically more correct than fixing them to the maximum likelihood values obtained from the SPNA (as it is usually done in a PTA inference for a GWB), and will result in slightly wider posteriors for the GWB hyperparameters too. A tutorial about reproducing Fig. 1 can be found at [52].

From Fig. 1, we can also notice that the obtained posteriors for the RN and DM hyperparameters are highly covariant. In Appendix C, we discuss a possible method to capture the covariance between RN and other signals using principal component analysis (PCA) principles. Being able to discriminate between RN and DM variations confidently would allow us to include the DM hyperparameters in *Step 1*.

In this Section, we showed the results obtained for the pulsar J1738+0333. We also tested all the other 24 pulsars of the EPTA DR2new and always obtained perfect agreement between the RN and DM hyperparameters posteriors obtained with the time-domain likelihood and the regularized likelihood in Fourier domain. For the case of J1600-3053, the EPTA DR2new noise analysis [50] found evidence for an additional chromatic noise component. This is also supported by our method and can be sampled for in *Step 2*. In the case of the DM dip found in the J1713+0747 data, this deterministic signal can also be included in our model as one of the signals that get marginalized over after *Step 1*.

### B. GWB search

In this Section, we present the results obtained carrying out a GWB search on EPTA DR2new dataset with our regularized likelihood in Fourier domain (Eq. 18) and compare them with the results obtained with the

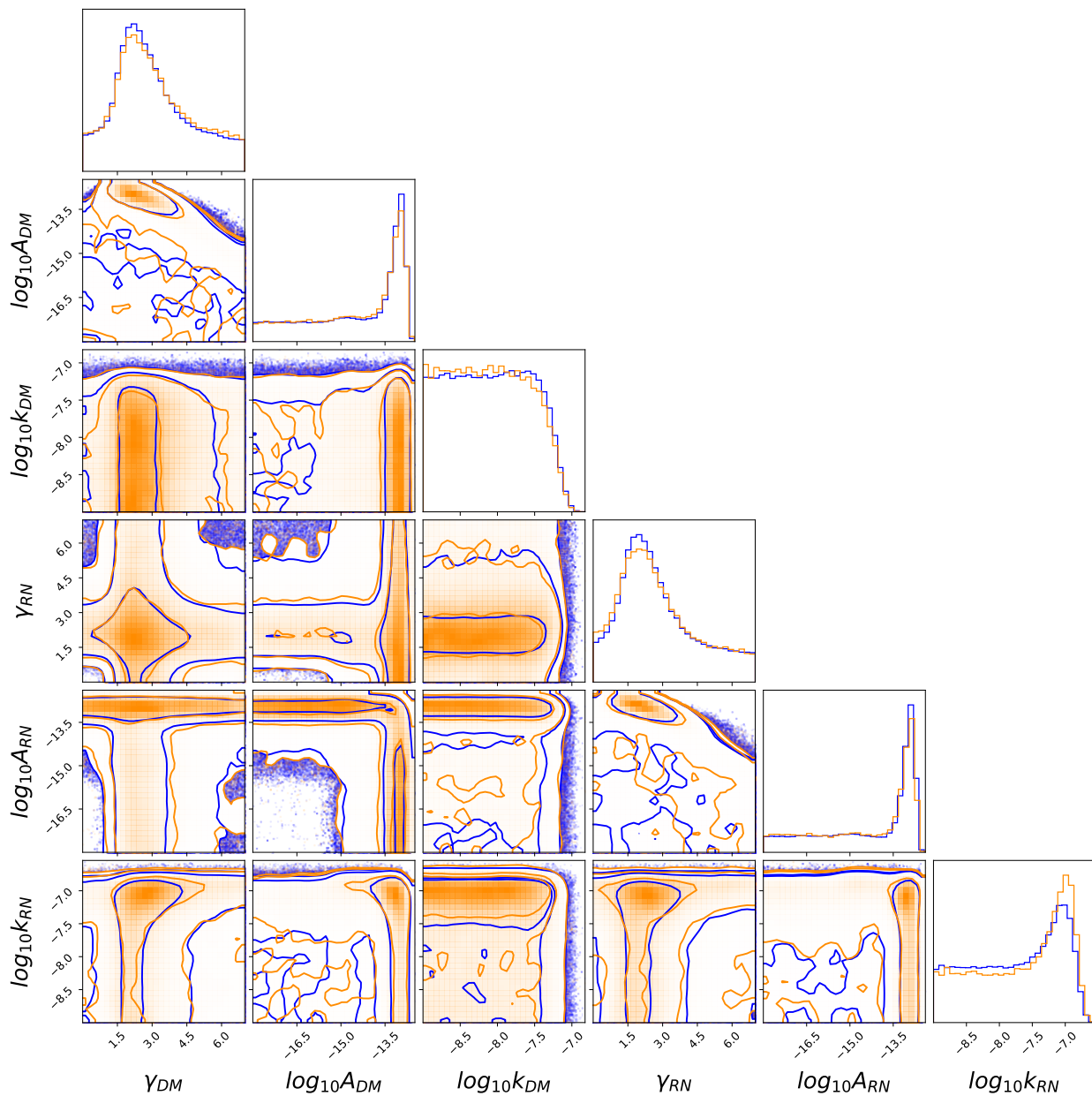


Figure 1. Posteriors for J1738+0333 noise analysis. The orange posteriors are obtained for an inference run over the Gaussian noise processes with the regularized likelihood in Fourier domain; the blue ones come from a full SPNA over all the noise processes using the time-domain likelihood.

standard time-domain likelihood (Eq. 11)<sup>2</sup>. As expected, the two methods are perfectly equivalent (see posteriors in Fig. 2: the blue posteriors are obtained from the standard Bayesian inference study in the time

domain (Sec. IIB), while the orange posteriors are obtained with the Fourier-domain method described in Sec. IIC).

To obtain the posteriors in Fig. 2, we first carried out *Step 1* analysis individually on all the 25 pulsars of EPTA DR2new. For each of them, we obtained samples of the white noise parameters (EFAC and EQUAD specific for each observing system). At the same time,

<sup>2</sup> The results of the GWB search on the EPTA DR2new dataset carried out by the EPTA collaboration can be found in [4, 53].

the RN and DM variations hyperparameters were fixed to  $\log_{10}A = -12$ ,  $\gamma = 5$ , and  $\log_{10}k = -5$ . RN and DM noise processes are modeled over, respectively, 30 and 100 frequency bins for all pulsars. Additionally, according to the results of the customized noise analysis carried out in [50], an exponential DM dip (deterministic signal) was added for J1713+0747 and sampled over in *Step 1*. Furthermore, the noise model of J1600-3053 includes an additional chromatic noise signal modeled as a Gaussian process (with a flat-tail power-law spectrum) and whose hyperparameters are fixed in this first analysis to  $\log_{10}A = -12$ ,  $\gamma = 5$  and  $\log_{10}k = -5$ .

From the results of those single pulsar analyzes, we obtain an estimate of  $\Sigma_0$  and  $\hat{\mathbf{a}}_0$ , as described in Eq. 20. We now have all the elements to use the posterior distribution function of Eq. 18 to conduct an inference run over all the pulsars' Gaussian noise processes and the GWB hyperparameters. We assumed the GWB to be stationary, Gaussian and with a power-law spectrum. The GWB amplitude and slope posteriors are shown in Fig. 2 (orange curve).

From Fig. 2 it is clear that the results obtained with the time-domain likelihood and the regularized likelihood in Fourier domain are equivalent. However, the way white noise is included in the analysis is different. In the time-domain analysis, the white noise parameters are fixed to the maximum likelihood values obtained in the SPNA runs. In the Fourier-domain analysis, instead, we marginalized over the white noise parameters. Furthermore, we are able to marginalize over other deterministic signals, like exponential DM dips.

The code used to produce the posteriors in Fig. 2 can be found at [52].

### C. Future applications: Gamma-ray PTA

In the first Gamma-ray PTA data release [26], the results from two different strategies to fit for the timing model and RN parameters from gamma-ray pulsars' data were presented. The first method is the same one used for radio pulsars: a continuous observation of the pulsar is “folded” and averaged over the pulsar spin period; the resulting peak is cross-correlated with a template to obtain a TOA. While this method is very efficient for radio pulsars, for many of the observed gamma-ray millisecond pulsars, the limited *exposure* (collecting area per time) would make it necessary to fold many months of data in order to build a constrained TOA. An alternative method is the photon-to-photon approach [30]. In this case, each photon gets assigned a probability that it belongs or not to the pulse template of that pulsar; those probabilities are used as weights in the pulsar likelihood to determine the timing model parameters. Contrarily to the likelihood function used for radio PTA (Eq. 11), this likelihood is not a Gaussian.

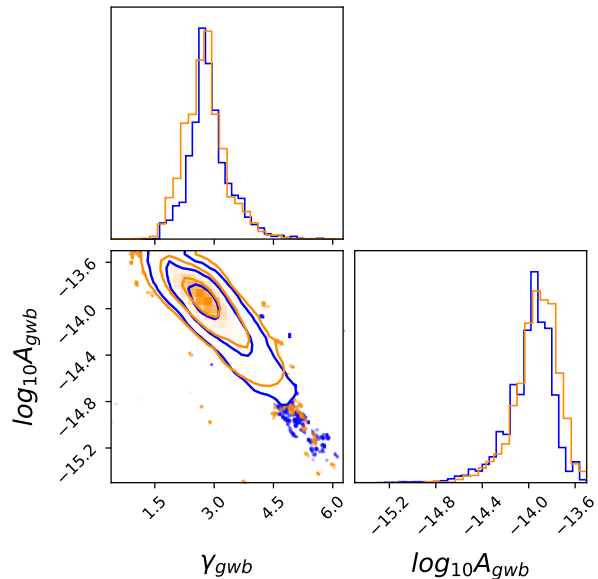


Figure 2. Posteriors for the GWB hyperparameters obtained from the 25 pulsars of the EPTA DR2new dataset. The orange posteriors are obtained with the regularized likelihood in Fourier domain (the WN and DM dip parameters are marginalized over); the blue ones are obtained with the time-domain likelihood (the WN parameters are fixed).

Thus, it can be computed for any sample of values for the timing model and signal processes parameters, but it is not possible to analytically marginalize over any parameter. [Note that, in standard radio PTA inference, we *always* marginalize over the timing model parameters and the Fourier coefficients used to describe the included Gaussian processes.]

In Gamma-ray PTA pulsar noise inference, the parameters searched for are both the timing model parameters and the Fourier coefficients of the waveform describing the Gaussian processes involved (remember that, in this case, there is no DM dispersion effect). More details about this type of analysis can be found at [26, 54].

To date, the photon-to-photon approach was missing a method to look for correlated signals among different pulsars. Previous analyses [31] have only produced upper limits on the amplitude of a common red signal, where no correlation information was included. One of the main motivations for this work was to derive a PTA likelihood function that could be applied to Gamma-ray PTA data obtained with the photon-to-photon approach. The posterior samples of the Fourier coefficients (describing the Gaussian signal processes in each pulsars' data) can be used as input for our regularized likelihood (Eq. 18) when looking at the whole

array. We leave this analysis for future work.

#### IV. CONCLUSIONS

We presented a regularized formulation of the PTA likelihood in Fourier domain (Eq. 18) and showed results for both single pulsar noise analysis (Fig. 1) and GWB searches (Fig. 2) using the EPTA DR2new dataset [49]. We proved that our formulation is analytically equivalent to the time-domain likelihood (Eq. 11) when the white noise (and deterministic signals) parameters are held fixed.

Our regularized likelihood in Fourier domain can be seen as the product of two terms (Eq. 14): (a) a Gaussian distribution in the Fourier coefficients  $\mathbf{a}$ , describing all the Gaussian processes included in the model, which depend on a given set of model hyperparameters  $\rho_0$ ; (b) a reweighting term consisting in the ratio between the prior probabilities evaluated for a general sample of the model hyperparameters  $\rho$  and for  $\rho = \rho_0$ . (See Sec. II C for more details.)

We identify two main advantages coming from using our regularized likelihood function (Eq. 18):

(i) It allows the splitting of the GWB inference on a PTA dataset in a two-step analysis. *Step 1* consists of conducting inference on the parameters of those signals not covariant with a GWB (white noise and deterministic signals); each pulsar is analyzed individually. *Step 2* analyses the whole array simultaneously and produces inference on the hyperparameters of the GWB and signals covariant with it (RN, DM variations, etc.). All the parameters investigated in *Step 1* are marginalized over.

(ii) It favors the immediate inclusion of gamma-

ray data in the PTA dataset alongside the radio timing data without waiving the complexity and pulsar-specificity of the radio noise models. Analyzing gamma-ray data with the *photon-to-photon* approach [30], we evaluate the pulse phase at each individual photon-time and compare it with a template. We can then write a Poisson likelihood for this data that fits both the timing model parameters and the Fourier coefficients of the involved noise components (modeled as Gaussian processes, [54]). The resulting Fourier coefficients become the input of our PTA likelihood (Eq. 18) when carrying out inference studies on the whole array. Thus, this regularized likelihood can be applied to both radio and gamma-ray data, independently of the software and models used to obtain the Fourier coefficients from the raw data. This opens the way for possible direct comparisons between the results from the two datasets.

*Data and code availability:* The scripts used to produce the figures in this paper can be found at [52]. The EPTA DR2new dataset is available on zenodo [42].

#### ACKNOWLEDGMENTS

We thank Colin Clark for insightful discussions about gamma-ray pulsar observations and data analysis.

This work was supported by the Max Planck Gesellschaft (MPG) and the ATLAS cluster computing team at AEI Hannover.

We also made use of `numpy` [55], `matplotlib` [56], `corner plot` [57], `scipy` [43], `tempo2` [34, 35], `libstempo` [58], `enterprise` [36], `PTMCMCSampler` [51] and `la_forge` [59].

- 
- [1] D. R. Lorimer and M. Kramer, *Handbook of Pulsar Astronomy*, Vol. 4 (2004).
- [2] R. W. Hellings and G. S. Downs, *The Astrophysical Journal Letters* **265**, L39 (1983).
- [3] H. Xu, S. Chen, *et al.* (The CPTA Collaboration), *Research in Astronomy and Astrophysics* **23**, 075024 (2023).
- [4] J. Antoniadis *et al.* (EPTA and InPTA Collaborations), *Astronomy & Astrophysics* **678**, A50 (2023).
- [5] G. Agazie *et al.* (The NANOGrav Collaboration), *The Astrophysical Journal Letters* **951**, L8 (2023).
- [6] D. J. Reardon, A. Zic, *et al.* (The PPTA Collaboration), *The Astrophysical Journal Letters* **951**, L6 (2023).
- [7] M. T. Miles, R. M. Shannon, D. J. Reardon, M. Bailes, D. J. Champion, M. Geyer, P. Gitika, K. Grunthal, M. J. Keith, M. Kramer, A. D. Kulkarni, R. S. Nathan, A. Parthasarathy, J. Singha, G. Theureau, E. Thrane, F. Abbate, S. Buchner, A. D. Cameron, F. Camilo, B. E. Moreschi, G. Shaifullah, M. Shamohammadi, A. Possenti, and V. V. Krishnan, *Monthly Notices of the Royal Astronomical Society*, stae2571 (2024), <https://academic.oup.com/mnras/advance-article-pdf/doi/10.1093/mnras/stae2571/60898823/stae2571.pdf>.
- [8] G. Agazie *et al.* (The International Pulsar Timing Array Collaboration), Comparing recent pta results on the nanohertz stochastic gravitational wave background (2023), arXiv:2309.00693 [astro-ph.HE].
- [9] J. P. W. Verbiest, S. J. Vigeland, N. K. Porayko, S. Chen, and D. J. Reardon, *Results Phys.* **61**, 107719 (2024), arXiv:2404.19529 [astro-ph.HE].
- [10] M. Rajagopal and R. W. Romani, *Astrophys. J.* **446**, 543 (1995), arXiv:astro-ph/9412038 [astro-ph].

- [11] A. H. Jaffe and D. C. Backer, *Astrophys. J.* **583**, 616 (2003), arXiv:astro-ph/0210148 [astro-ph].
- [12] J. S. B. Wyithe and A. Loeb, *Astrophys. J.* **590**, 691 (2003), arXiv:astro-ph/0211556 [astro-ph].
- [13] A. Sesana, A. Vecchio, and C. N. Colacino, *Monthly Notices of the Royal Astronomical Society* **390**, 192 (2008), <https://academic.oup.com/mnras/article-pdf/390/1/192/2959688/mnras0390-0192.pdf>.
- [14] P. A. Rosado, A. Sesana, and J. Gair, *Monthly Notices of the Royal Astronomical Society* **451**, 2417 (2015).
- [15] T. Damour and A. Vilenkin, *Phys. Rev. Lett.* **85**, 3761 (2000), arXiv:gr-qc/0004075 [gr-qc].
- [16] H. Quelquejay Leclere, P. Auclair, S. Babak, A. Chalumeau, D. A. Steer, J. Antoniadis, A.-S. B. Nielsen, C. Bassa, A. Berthreau, M. Bonetti, E. Bortolas, P. Brook, M. Burgay, R. Caballero, D. Champion, S. Chanlaridis, S. Chen, I. Cognard, G. Desvignes, M. Falxa, R. Ferdman, A. Franchini, J. Gair, B. Goncharov, E. Graikou, J.-M. Grießmeier, L. Guillemot, Y. Guo, H. Hu, F. Iraci, D. Izquierdo-Villalba, J. Jang, J. Jawor, G. Janssen, A. Jessner, R. Karuppusamy, E. Keane, M. Keith, M. Kramer, M. Krishnakumar, K. Lackeos, K. Lee, K. Liu, Y. Liu, A. Lyne, J. McKee, R. Main, M. Mickaliger, I. Nițu, A. Parthasarathy, B. Perera, D. Perrodin, A. Petiteau, N. Porayko, A. Possenti, A. Samajdar, S. Sanidas, A. Sesana, G. Shaifullah, L. Speri, R. Spiewak, B. Stappers, S. Susarla, G. Theureau, C. Tiburzi, E. van der Wateren, A. Vecchio, V. V. Krishnan, J. Wang, L. Wang, and Z. Wu, *Physical Review D* **108**, 10.1103/physrevd.108.123527 (2023).
- [17] K. Tomita, *Progress of Theoretical Physics* **37**, 831 (1967).
- [18] S. Matarrese, O. Pantano, and D. Saez, *Phys. Rev. D* **47**, 1311 (1993).
- [19] A. Kosowsky, M. S. Turner, and R. Watkins, *Phys. Rev. D* **45**, 4514 (1992).
- [20] M. Hindmarsh, S. J. Huber, K. Rummukainen, and D. J. Weir, *Phys. Rev. Lett.* **112**, 041301 (2014), arXiv:1304.2433 [hep-ph].
- [21] N. Bartolo, S. Matarrese, A. Riotto, and A. Väihkönen, *Phys. Rev. D* **76**, 061302 (2007), arXiv:0705.4240 [astro-ph].
- [22] L. A. Boyle and A. Buonanno, *Phys. Rev. D* **78**, 043531 (2008), arXiv:0708.2279 [astro-ph].
- [23] L. Sorbo, *Journal of Cosmology and Astroparticle Physics* **2011** (06), 003–003.
- [24] J. Antoniadis *et al.* (EPTA and InPTA Collaborations), The second data release from the european pulsar timing array: V. implications for massive black holes, dark matter and the early universe (2023), arXiv:2306.16227 [astro-ph.CO].
- [25] A. Afzal *et al.* (The NANOGrav Collaboration), *The Astrophysical Journal Letters* **951**, L11 (2023).
- [26] M. Ajello, W. B. Atwood, L. Baldini, J. Ballet, *et al.*, *Science* **376**, 521–523 (2022).
- [27] P. Bickel, B. Kleijn, and J. Rice, *The Astrophysical Journal* **685**, 384 (2008).
- [28] M. Kerr, *The Astrophysical Journal* **732**, 38 (2011).
- [29] P. Bruel, *Astronomy & Astrophysics* **622**, A108 (2019).
- [30] M. Kerr, *The Astrophysical Journal* **885**, 92 (2019).
- [31] M. Kerr, A. Parthasarathy, and T. Cromartie (Large Area Telescope), *PoS ICRC2023*, 1595 (2023).
- [32] J. Luo, S. Ransom, P. Demorest, P. S. Ray, A. Archibald, M. Kerr, R. J. Jennings, M. Bachetti, R. van Haasteren, C. A. Champagne, J. Colen, C. Phillips, J. Zimmerman, K. Stovall, M. T. Lam, and F. A. Jenet, *The Astrophysical Journal* **911**, 45 (2021).
- [33] A. Susobhanan, D. Kaplan, A. Archibald, J. Luo, P. Ray, T. Pennucci, S. Ransom, G. Agazie, W. Fiore, B. Larsen, P. O’Neill, R. van Haasteren, A. Anumalapudi, M. Bachetti, D. Bhakta, C. Champagne, H. T. Cromartie, P. Demorest, R. Jennings, M. Kerr, S. Levina, A. McEwen, B. Shapiro-Albert, and J. Swiggum, *Pint: Maximum-likelihood estimation of pulsar timing noise parameters* (2024), arXiv:2405.01977 [astro-ph.IM].
- [34] G. B. Hobbs, R. T. Edwards, and R. N. Manchester, *Monthly Notices of the Royal Astronomical Society* **369**, 655 (2006).
- [35] R. T. Edwards, G. B. Hobbs, and R. N. Manchester, *Monthly Notices of the Royal Astronomical Society* **372**, 1549 (2006), <https://academic.oup.com/mnras/article-pdf/372/4/1549/4012423/mnras0372-1549.pdf>.
- [36] J. A. Ellis, M. Vallisneri, S. R. Taylor, and P. T. Baker, ENTERPRISE: Enhanced Numerical Toolbox Enabling a Robust Pulsar Inference Suite, *Astrophysics Source Code Library*, record ascl:1912.015 (2019), ascl:1912.015.
- [37] R. N. Caballero, K. J. Lee, L. Lentati, G. Desvignes, D. J. Champion, J. P. W. Verbiest, G. H. Janssen, B. W. Stappers, M. Kramer, P. Lazarus, A. Possenti, C. Tiburzi, D. Perrodin, S. Osłowski, S. Babak, C. G. Bassa, P. Brem, M. Burgay, I. Cognard, J. R. Gair, E. Graikou, L. Guillemot, J. W. T. Hessels, R. Karuppusamy, A. Lassus, K. Liu, J. McKee, C. M. F. Mingarelli, A. Petiteau, M. B. Purver, P. A. Rosado, S. Sanidas, A. Sesana, G. Shaifullah, R. Smits, S. R. Taylor, G. Theureau, R. van Haasteren, and A. Vecchio, *Monthly Notices of the Royal Astronomical Society* **457**, 4421 (2016), <https://academic.oup.com/mnras/article-pdf/457/4/4421/18511407/stw179.pdf>.
- [38] L. Lentati, P. Alexander, M. P. Hobson, S. Taylor, J. Gair, S. T. Balan, and R. van Haasteren, *Physical Review D* **87**, 10.1103/physrevd.87.104021 (2013).
- [39] R. van Haasteren, Y. Levin, P. McDonald, and T. Lu, *Monthly Notices of the Royal Astronomical Society* **395**, 1005–1014 (2009).
- [40] R. van Haasteren and Y. Levin, *Monthly Notices of the Royal Astronomical Society* **428**, 1147–1159 (2012).
- [41] R. van Haasteren and M. Vallisneri, *Physical Review D* **90**, 10.1103/physrevd.90.104012 (2014).
- [42] J. Antoniadis *et al.* (EPTA and InPTA Collaborations), 10.5281/zenodo.8164425 (2023).
- [43] P. Virtanen, R. Gommers, T. E. Oliphant, M. Haberland, T. Reddy, D. Cournapeau, E. Burovski, P. Peterson, W. Weckesser, J. Bright, S. J. van der Walt, M. Brett, J. Wilson, K. J. Millman, N. Mayorov, A. R. J. Nelson, E. Jones, R. Kern, E. Larson, C. J. Carey, Í. Polat, Y. Feng, E. W. Moore, J. VanderPlas,

- D. Laxalde, J. Perktold, R. Cimrman, I. Henriksen, E. A. Quintero, C. R. Harris, A. M. Archibald, A. H. Ribeiro, F. Pedregosa, P. van Mulbregt, and SciPy 1.0 Contributors, *Nature Methods* **17**, 261 (2020).
- [44] M. Vallisneri and R. van Haasteren, *Monthly Notices of the Royal Astronomical Society*, stx069 (2017).
- [45] N. Laal, W. G. Lamb, J. D. Romano, X. Siemens, S. R. Taylor, and R. van Haasteren, *Physical Review D* **108**, 10.1103/physrevd.108.063008 (2023).
- [46] N. Laal, S. R. Taylor, R. van Haasteren, W. G. Lamb, and X. Siemens, Solving the pta data analysis problem with a global gibbs scheme (2024), arXiv:2410.11944 [astro-ph.IM].
- [47] S. R. Taylor, J. Simon, L. Schult, N. Pol, and W. G. Lamb, *Physical Review D* **105**, 10.1103/physrevd.105.084049 (2022).
- [48] J. S. Hazboun, J. Simon, S. R. Taylor, M. T. Lam, S. J. Vigeland, K. Islo, J. S. Key, Z. Arzoumanian, P. T. Baker, A. Brazier, P. R. Brook, S. Burke-Spolaor, S. Chatterjee, J. M. Cordes, N. J. Cornish, F. Crawford, K. Crowter, H. T. Cromartie, M. DeCesar, P. B. Demorest, T. Dolch, J. A. Ellis, R. D. Ferdman, E. Ferrara, E. Fonseca, N. Garver-Daniels, P. Gentile, D. Good, A. M. Holgado, E. A. Huerta, R. Jennings, G. Jones, M. L. Jones, A. R. Kaiser, D. L. Kaplan, L. Z. Kelley, T. J. W. Lazio, L. Levin, A. N. Lommen, D. R. Lorimer, J. Luo, R. S. Lynch, D. R. Madison, M. A. McLaughlin, S. T. McWilliams, C. M. F. Mingarelli, C. Ng, D. J. Nice, T. T. Pennucci, N. S. Pol, S. M. Ransom, P. S. Ray, X. Siemens, R. Spiewak, I. H. Stairs, D. R. Stinebring, K. Stovall, J. Swiggum, J. E. Turner, M. Vallisneri, R. van Haasteren, C. A. Witt, and W. W. Zhu, *Astrophys. J.* **890**, 108 (2020), arXiv:1909.08644 [astro-ph.HE].
- [49] J. Antoniadis *et al.* (EPTA and InPTA Collaborations), *A&A* **678**, A48 (2023).
- [50] J. Antoniadis *et al.* (EPTA and InPTA Collaborations), *A&A* **678**, A49 (2023).
- [51] J. Ellis and R. van Haasteren, jellis18/ptmcmcsampler: Official release (2017).
- [52] [https://github.com/serevaltolina/PTA\\_FourierLikelihood](https://github.com/serevaltolina/PTA_FourierLikelihood).
- [53] B. Goncharov and S. Sardana, Ensemble noise properties of the european pulsar timing array (2024), arXiv:2409.03661 [astro-ph.HE].
- [54] T. Thongmearkom, C. J. Clark, R. P. Breton, M. Burgay, L. Nieder, P. C. C. Freire, E. D. Barr, B. W. Stappers, S. M. Ransom, S. Buchner, F. Calore, D. J. Champion, I. Cognard, J. M. Grießmeier, M. Kramer, L. Levin, P. V. Padmanabh, A. Possenti, A. Ridolfi, V. V. Krishnan, and L. Vleeschower, A targeted radio pulsar survey of redback candidates with meerkat (2024), arXiv:2403.09553 [astro-ph.HE].
- [55] C. R. Harris, K. J. Millman, S. J. van der Walt, R. Gommers, P. Virtanen, D. Cournapeau, E. Wieser, J. Taylor, S. Berg, N. J. Smith, R. Kern, M. Picus, S. Hoyer, M. H. van Kerkwijk, M. Brett, A. Haldane, J. F. del Río, M. Wiebe, P. Peterson, P. Gérard-Marchant, K. Sheppard, T. Reddy, W. Weckesser, H. Abbasi, C. Gohlke, and T. E. Oliphant, *Nature* **585**, 357 (2020).
- [56] J. D. Hunter, *Computing in Science & Engineering* **9**, 90 (2007).
- [57] D. Foreman-Mackey, *The Journal of Open Source Software* **1**, 24 (2016).
- [58] M. Vallisneri, libstempo: Python wrapper for Tempo2, *Astrophysics Source Code Library*, record ascl:2002.017 (2020), ascl:2002.017.
- [59] J. S. Hazboun, La forge (2020).
- [60] W. G. Lamb, S. R. Taylor, and R. van Haasteren, *Physical Review D* **108**, 10.1103/physrevd.108.103019 (2023).
- [61] J. W. Cooley and J. W. Tukey, *Mathematics of Computation* **19**, 297 (1965), 2003354.
- [62] C. M. Bishop and H. Bishop, *Deep Learning: Foundations and Concepts* (Springer International Publishing, Cham, 2024).
- [63] W. Coles, G. Hobbs, D. J. Champion, R. N. Manchester, and J. P. W. Verbiest, *Monthly Notices of the Royal Astronomical Society* **418**, 561 (2011).
- [64] R. Vershynin, *High-Dimensional Probability: An Introduction with Applications in Data Science*, Cambridge Series in Statistical and Probabilistic Mathematics (Cambridge University Press, 2018).
- [65] I. Jolliffe and J. Cadima, *Philosophical Transactions of the Royal Society A: Mathematical, Physical and Engineering Sciences* **374**, 20150202 (2016).

## Appendix A: Fourier coefficients sampling and numerical resolution problems

The main idea that inspired our paper is that of the Fourier transform: our goal was to carry out an analysis similar to a Fourier transform, so that we could work with the Fourier-transformed data. Such an approach would make it easier to combine radio, gamma-ray, or other types of pulsar timing data. Moreover, this could then potentially be done on a per-pulsar basis, after which a full PTA analysis would be done on the data product of the per-pulsar analysis. The methods presented by [60] can be seen as such an effort. However, this is difficult to achieve in full generality, because the pulsar timing data is complex: the data is sampled irregularly, data products are not the same for radio/gamma-ray data, the signals of interest are very low-frequency, and we have to take into account the effects of the timing model. Let us briefly review the Fourier transform here in order to motivate our regularization technique in detail.

### 1. Regularization

In classical time-series analysis, the data can be converted from the time-domain to the Fourier domain by the Discrete Fourier Transform (DFT): an invertible linear transformation of the data which we can write as:

$$\delta t = F \tilde{\delta} t, \quad (\text{A1})$$

where  $\tilde{\delta t}$  is the DFT of the data  $\delta t$ . In Eq. A1, the transformation matrix  $F$  has complex exponential basis functions as its columns, with frequencies being multiples of the fundamental harmonic of the time-series. Fast implementations of Eq. A1 exist in the form of the Fast Fourier Transform [61].

The DFT is an invertible transformation, meaning that the columns of  $F$  constitute a complete basis for our time series  $\delta t$ . This also means that both the signal and the noise are fully represented by  $\tilde{\delta t}$ . Often times in signal processing, including in PTA data analysis, the goal is to capture the underlying processes of interest, not the noise. Thinking of  $\tilde{\delta t}$  from that perspective, the fact that the DFT is invertible means that we are *overfitting* the data. Overfitting is a consequence of having too many degrees of freedom in the model, resulting in capturing not only the processes of interest, but also the noise. Common solutions to overfitting include (1) reducing the degrees of freedom in the model, or (2) regularizing the model using constraints. In the machine learning literature, many regularization techniques have been developed over the past decades [62].

In pulsar timing, it is customary (for computational reasons) to use fewer frequencies, meaning that  $F$  becomes a non-square matrix with fewer columns than rows. This means that the linear system of Eq. A1 can be interpreted as an over-determined system, and solutions like those obtained through least-squares optimization can be used. As hinted at above, reducing the number of frequencies is a regularization technique, because it removes degrees of freedom of the model. Indeed, if the higher frequencies are omitted from the model, the model should only capture trends of lower frequency.

In pulsar timing the data is sampled irregularly and quadratic spindown always needs to be taken into account when doing spectral analysis [63]. The result is that all Fourier transform elements are covariant. Moreover, there is degeneracy between the quadratic spindown parameters and the lowest frequency Fourier coefficients if we allow all those parameters to be free unconstrained in the model. This degeneracy can be broken by placing a constraint on the Fourier coefficients. We do this by placing a Gaussian prior on the Fourier coefficients. This regularizes the posterior distribution and breaks the degeneracy with the timing model. And, because we have an *analytical* description of the Gaussian prior, we can *undo* it at a later stage in the analysis without running into numerical issues stemming from finite number of samples (a usual problem with resampling approaches). This approach retains all information in the data.

## 2. Numerical resolution

The  $\rho_0$  define the regularization of the Fourier coefficients that we use in Section II C. Care needs to be taken in choosing the values of  $\rho_0$  so that numerical issues like under/overflow and roundoff errors are avoided. The distribution of Fourier coefficients is obtained by estimating directly its mean and variance, rather than computing them from  $\mathbf{a}$  samples. The  $\Sigma_0$  matrix is evaluated from the distribution of  $\Sigma_{0i}$  matrices, all of which are obtained from a given set of samples of all the hyperparameters and, thus, are not singular. In our analysis, we used one thousand of  $\Sigma_{0i}$  samples to compute  $\Sigma_0$  using the update formula in Eq. 20. This resulted in an accuracy on the estimator the individual elements of the covariance matrix of the order of 0,04%.

An alternative method to estimate the covariance matrix  $\Sigma_0$  would be to compute it directly from a set of samples of the Fourier coefficients  $\mathbf{a}$  describing the Gaussian processes involved in the model (we use that approach in Appendix C, see Eq. C10 and C11). This may lead to numerical resolution problems when computing the inverse of  $\Sigma'_0$ .

The  $\Sigma'_0$  matrix is characterized by both very large and very small eigenvalues. Even if most of the covariance information lies in the larger eigenvalues, the small eigenvalues are necessary to guarantee the matrix is positive definite.  $\Sigma'_0$  has a very high condition number and is a so-called *ill-conditioned* matrix. To guarantee numerical stability, the number of samples should be at least of the same order of magnitude as the product between the matrix's condition number and the number of features  $m'$  ( $\Sigma'_0$  is a  $(m' \times m')$  matrix) [64].

The condition number of  $\Sigma'_0$  can be reduced for optimal choices of the  $\rho_0$  values to which the Gaussian process hyperparameters are fixed. From looking at the reweighting term in

$$\begin{aligned} p(\mathbf{a}_{\text{RN}}, \boldsymbol{\rho}_{\text{RN}}, \mathbf{a}_{\text{DM}}, \boldsymbol{\rho}_{\text{DM}} | \boldsymbol{\theta}, \delta t) = & \\ p(\mathbf{a}_{\text{RN}}, \mathbf{a}_{\text{DM}} | \boldsymbol{\theta}, \boldsymbol{\rho}_{\text{RN}_0}, \boldsymbol{\rho}_{\text{DM}_0}) & \\ \times p(\mathbf{a}_{\text{RN}} | \boldsymbol{\rho}_{\text{RN}}) p(\mathbf{a}_{\text{DM}} | \boldsymbol{\rho}_{\text{DM}}) & \quad (\text{A2}) \\ \div \left[ p(\mathbf{a}_{\text{RN}} | \boldsymbol{\rho}_{\text{RN}_0}) p(\mathbf{a}_{\text{DM}} | \boldsymbol{\rho}_{\text{DM}_0}) \right], & \end{aligned}$$

it is clear that the distribution at the denominator has to be wider than the condition number at the numerator, such that the ratio is still a Gaussian distribution. Thus, the  $\rho_0$  values should be chosen accordingly. Assuming a flat-tail power-law spectra for both RN and DM variations favors the stability of the algorithm. In fact, by comparing the periodograms (spectral density plots as a function of frequency) of those processes for different values of the  $\rho_0$  parameters, it becomes clear that the  $\log_{10} k_0$  is the real discriminant in this equation. In practice, for realistic PTA datasets, a value of  $\log_{10} k \in (-6, -3)$  should be enough to guarantee that

the denominator distribution is wider than the distribution at the numerator, making the posterior is normalizable. Although, the exact range is pulsar specific and depends on the observation cadence. Other potential solutions are standard matrix regularization or Cholesky rank-1 update algorithms.

### Appendix B: Covariance matrix update formula

In this Appendix, we derive the formula used to compute the variance  $\Sigma_0$  from the distribution of  $\Sigma_{0i}$  elements (Eq. 20). We start from a easier case, where we want to write the covariance matrix of a set of  $n + p$  samples ( $C_{n+p}$ ) as a function of the covariance matrices  $C_n$  and  $C_p$  (obtained considering, respectively, only the first  $n$  and the last  $p$  samples), and then generalize

the result to obtain Eq. 20.

Given  $n$  independent observations (samples) of the set of parameters  $\mathbf{x}$ , where  $\mathbf{x} = (x_1, x_2, \dots, x_m)$ , the covariance matrix  $C_n \in \mathcal{R}^{n \times m}$  is defined as

$$\begin{aligned} C_n &\equiv \frac{1}{n-1} \sum_{i=1}^n (\mathbf{x}_i - \hat{\mathbf{x}}_n)(\mathbf{x}_i - \hat{\mathbf{x}}_n)^T \\ &= \frac{1}{n-1} \left[ \sum_{i=1}^n \mathbf{x}_i \mathbf{x}_i^T - \sum_{i=1}^n \mathbf{x}_i \hat{\mathbf{x}}_n^T - \hat{\mathbf{x}}_n \left( \sum_{i=1}^n \mathbf{x}_i \right)^T + n \hat{\mathbf{x}}_n \hat{\mathbf{x}}_n^T \right] \\ &= \frac{1}{n-1} \left[ \sum_{i=1}^n \mathbf{x}_i \mathbf{x}_i^T - n \hat{\mathbf{x}}_n \hat{\mathbf{x}}_n^T \right], \end{aligned} \tag{B1}$$

where  $\hat{\mathbf{x}}_n = \sum_i \mathbf{x}_i / n$  is the mean over the  $n$  samples of  $\mathbf{x}$ . Note that, by definition, when  $n = 1$  the fraction in Eq. B1 becomes simply  $1/n = 1$ .

---

Consider now  $n + p$  samples of  $\mathbf{x}$ . The mean  $\hat{\mathbf{x}}_{n+p}$  can be rewritten as

$$\hat{\mathbf{x}}_{n+p} = \frac{1}{n+p} \left( \sum_{i=1}^n \mathbf{x}_i + \sum_{j=1}^p \mathbf{x}_j \right) = \frac{1}{n+p} (n \hat{\mathbf{x}}_n + p \hat{\mathbf{x}}_p). \tag{B2}$$

From Eq. B1, it is immediate to see that the covariance matrix  $C_{n+p}$  is defined as:

$$C_{n+p} = \frac{1}{n+p-1} \left[ \sum_{i=1}^{n+p} \mathbf{x}_i \mathbf{x}_i^T - \sum_{i=1}^{n+p} \mathbf{x}_i \hat{\mathbf{x}}_{n+p}^T - \hat{\mathbf{x}}_{n+p} \left( \sum_{i=1}^{n+p} \mathbf{x}_i \right)^T + (n+p) \hat{\mathbf{x}}_{n+p} \hat{\mathbf{x}}_{n+p}^T \right]. \tag{B3}$$

Dividing the sums  $\sum^{n+p} = \sum^n + \sum^p$  and using Eq. B2, we can rewrite Eq. B3 as a function of the mean and covariance of the two separate  $n$  and  $p$  sample sets:

$$C_{n+p} = \frac{1}{n+p-1} \left[ (n-1) C_n + (p-1) C_p + n \hat{\mathbf{x}}_n \hat{\mathbf{x}}_n^T + p \hat{\mathbf{x}}_p \hat{\mathbf{x}}_p^T - (n+p) \hat{\mathbf{x}}_{n+p} \hat{\mathbf{x}}_{n+p}^T \right] \tag{B4}$$

independently of the values of  $n$  and  $p$ .

This can be generalized to the case of  $N$  sets of  $n_k$  samples with means  $\hat{\mathbf{x}}_k$  and covariances  $C_k$  ( $k = 1, \dots, N$ ). The total covariance matrix  $C$  computed from all the  $N$  sets of samples can then be expressed as a function of the covariance matrices and means of the individual sets:

$$C = \frac{1}{\left( \sum_{k=1}^N n_k \right) - 1} \left[ \sum_{k=1}^N \left( (n_k - 1) C_k + n_k \hat{\mathbf{x}}_k \hat{\mathbf{x}}_k^T \right) - \left( \sum_{k=1}^N n_k \right) \hat{\mathbf{x}} \hat{\mathbf{x}}^T \right], \tag{B5}$$

where  $\hat{\mathbf{x}}$  is the mean over all the  $\sum n_k$  samples. This equation is exactly what is reported in Eq. 20 for the computation of the  $\Sigma_0$  matrix from the set of  $N_s$  matrices  $\Sigma_{0i}$ . Note that  $n_k = 1$  for each  $\Sigma_{0i}$  matrix (they are computed from a single sample of the noise hyperparameters).

### Appendix C: PCA approach to marginalize over DM variations

In this paper, we presented a regularized formulation of the PTA likelihood in Fourier-domain (Eq. 18) as an alternative to the commonly-used time-domain likelihood (Eq. 11). The computational cost of evalu-

---

ating the two likelihood functions is comparable: the dimensions of the involved matrices and the number of times those need to be inverted are almost identical. The number of free parameters is also similar. The advantage of using our regularized likelihood in Fourier domain is that deterministic signals (like, for example, DM dips) and other signals not covariant with the GWB

can be sampled over in *Step 1* of the analysis, and then marginalized over while carrying out the inference run over the whole array. This reduces the number of free parameters involved. (See Sec. II C for more details.)

In this Appendix, we investigate the possibility of including more signals in *Step 1* and further reduce the number of parameters when analyzing the full array (*Step 2*). The achromatic RN hyperparameters of the individual pulsars are strongly covariant with the GWB, defined as common spatially-correlated red noise, thus have to be sampled over alongside with the common process hyperparameters. The DM variations effect, instead, could theoretically be disentangled from the RN processes because of its frequency dependence. In fact, the DM variations signal (chromatic red noise) is due to the interaction of the pulsar radio emission with the ionized interstellar medium, the Solar System interplanetary medium and the Earth's ionosphere. These interactions lead to frequency-dependent delays in the observed TOAs (Eq. 5). Here, we describe a possible method to marginalize over the DM variations hyperparameters without losing information about their covariance with RN and GWB hyperparameters.

The main idea is to carry out a principal component analysis (PCA) to reduce the dimensionality of the problem and preserve information about the covariance between different hyperparameters. In this case, we want to capture the covariance between the Fourier coefficients describing the RN signal and the DM hyperparameters in a SPNA. Given a matrix  $X$  ( $n \times p$ ), each row of  $X$  can be mapped to a new row vector of length  $l < p$ . Thus, in matrix notation, we can write  $X' = XW_l$ , where  $X'$  ( $n \times l$ ) is the result of the PCA and contains the same covariance information as  $X$ . The matrix  $W_l$  ( $p \times l$ ) is the orthogonal linear transformation that maps each element of  $X$  in a new coordinate system of  $l$  principal components. Calling  $\mathbf{w}_j$  the  $l$ -dimensional unit vectors that constitute the row elements of  $W_l$ ,  $\mathbf{w}_1$  is

$$\begin{aligned} \mathbf{w}_1 &\equiv \operatorname{argmax}_{(\|\mathbf{w}\|=1)} \left\{ \|X\mathbf{w}\|^2 \right\} \\ &= \operatorname{argmax}_{(\|\mathbf{w}\|=1)} \left\{ \mathbf{w}^T X^T X \mathbf{w} \right\}. \end{aligned} \quad (\text{C1})$$

The  $k$ th component ( $k > 1$ ) can be computed by subtracting the  $k - 1$  principal components from  $X$ :

$$X_k = X - \sum_{j=1}^{k-1} X\mathbf{w}_j\mathbf{w}_j^T. \quad (\text{C2})$$

Thus, the  $k$ th weight vector is computed as

$$\mathbf{w}_k = \operatorname{argmax}_{(\|\mathbf{w}\|=1)} \left\{ \mathbf{w}^T X_k^T X_k \mathbf{w} \right\}. \quad (\text{C3})$$

The rows of the matrix  $W_l$  are the first  $l$  principal components  $\mathbf{w}_k$  ( $k = 1, \dots, l$ ). By construction,  $\mathbf{w}_k$  are also

the first  $l$  right singular vectors of  $X$  obtained by its singular value decomposition for the first  $l$  singular values ( $X = UCW^T$ , with  $C$  ( $n \times p$ ) rectangular diagonal matrix of the singular values,  $U$  ( $n \times n$ ) and  $W$  ( $p \times p$ ) contain, respectively, the left and right singular vectors). Since

$$X^T X = WC^T U^T UCW^T = W\tilde{C}^2 W^T, \quad (\text{C4})$$

where  $\tilde{C}^2 \equiv C^T C$ , the eigenvectors of  $X^T X$  (covariance matrix between observed correlated variables) are the right singular vectors of the matrix  $X$ . See [65] for more details on PCA approaches.

In the following subsection, we show how to apply this method to our case of interest: a SPNA where we want to reduce the dimensionality of the problem without waving information on the covariance between different noise hyperparameters.

### 1. Implementation: sampling over the Fourier coefficients

We describe here in detail the implementation of a PCA to marginalize over the DM variation hyperparameters when carrying out an inference run on PTA data. Notebook tutorials and the codes used to produce the figures in this Appendix are available at [52]. A complete summary of the notation is in Table I.

The main idea is to investigate the DM variations hyperparameters for each pulsar individually (include them in *Step 1*), and marginalize over them when analyzing the whole pulsars array without losing information on the covariance between the DM hyperparameters and the RN ones. In this scenario, Eq. 14 becomes:

$$\begin{aligned} p(\mathbf{a}_{\text{RN}}, \boldsymbol{\rho}_{\text{RN}}, \boldsymbol{\rho}_{\text{DM}} | \boldsymbol{\theta}, \delta\mathbf{t}) &= \\ p(\mathbf{a}_{\text{RN}} | \boldsymbol{\theta}, \boldsymbol{\rho}_{\text{DM}}, \boldsymbol{\rho}_{\text{RN}_0}) &\times \frac{p(\mathbf{a}_{\text{RN}} | \boldsymbol{\rho}_{\text{RN}}) p(\boldsymbol{\rho}_{\text{RN}})}{p(\mathbf{a}_{\text{RN}} | \boldsymbol{\rho}_{\text{RN}_0}) p(\boldsymbol{\rho}_{\text{RN}_0})}, \end{aligned} \quad (\text{C5})$$

where the DM hyperparameters are no longer included in the reweighting term. Introducing

$$\mathbf{x} \equiv \begin{bmatrix} \boldsymbol{\theta} \\ \boldsymbol{\rho}_{\text{DM}} \end{bmatrix}, \quad (\text{C6})$$

a PCA is applied to rewrite  $\mathcal{N}(\mathbf{a}_{\text{RN}} | \mathbf{x}, \boldsymbol{\rho}_{\text{RN}_0})$  as  $\mathcal{N}(\mathbf{a}_{\text{RN}} | \mathbf{x}', \boldsymbol{\rho}_{\text{RN}_0})$ , where  $\mathbf{x}'$  is an optimized linear combination of  $\boldsymbol{\theta}$  and  $\boldsymbol{\rho}_{\text{DM}}$  ( $\mathbf{x}$  is an  $m$ -dimensional vector,  $\mathbf{x}'$  is an  $m'$ -dimensional vector and  $m' < m$ ) that preserves the covariance between those parameters and  $\mathbf{a}_{\text{RN}}$ .

A normal distribution like  $\mathcal{N}(\mathbf{a} | \mathbf{x}, \boldsymbol{\rho}_{\text{RN}_0})$  is fully described by its mean  $\hat{\mathbf{a}}_0$  and variance  $\Sigma_0$ . The method described in Sec. II C directly estimates  $\hat{\mathbf{a}}_0$  and  $\Sigma_0$  from samples of the  $\boldsymbol{\theta}$  parameters (Eq. 19 and 20). The distribution  $\mathcal{N}(\mathbf{a}_{\text{RN}} | \mathbf{x}', \boldsymbol{\rho}_{\text{RN}_0})$  is associated to  $\hat{\mathbf{a}}'_0$  and  $\Sigma'_0$ .

These two quantities not only describe the distribution of the Fourier coefficients  $\mathbf{a}_{\text{RN}}$  when the RN hyperparameters are set to  $\boldsymbol{\rho}_{\text{RN}_0}$ , but also store information about their covariance with the DM hyperparameters  $\boldsymbol{\rho}_{\text{DM}}$ . We describe here how to obtain the best estimates for these quantities.

*Step 1* is analogous to *step 1* described in Sec. II C, with the exception that DM hyperparameters are not fixed to some values  $\boldsymbol{\rho}_{\text{DM}_0}$ , but sampled alongside the  $\boldsymbol{\theta}$  parameters. The next step would be to evaluate the  $\mathbf{x}'$  parameters in order to reduce the dimensionality of the problem without losing any information about the covariance between the hyperparameters of the involved signals.

We choose to evaluate the  $\mathbf{x}'$  parameters with a PCA. Thus,  $\mathbf{x}'$  are defined as a linear combination of the  $\boldsymbol{\theta}$  and  $\boldsymbol{\rho}_{\text{DM}}$  parameters, which optimally describes the covariance between them and the Fourier coefficients describing RN  $\mathbf{a}_{\text{RN}}$ . This information is encoded in the covariance matrix  $G$ :

$$G \equiv \langle \mathbf{a}_{\text{RN}} \mathbf{x}'^T \rangle. \quad (\text{C7})$$

In order to evaluate  $G$ , we need samples of the Fourier coefficients  $\mathbf{a}_{\text{RN}}$ . These can be drawn from the conditional distribution  $P(\mathbf{a}_{\text{RN}}|\mathbf{x}, \delta\mathbf{t})$  where the signal parameters  $\mathbf{x}$  come from the analysis in *Step 1*. This can be done through e.g. the package `la_forge` [59].<sup>3</sup>

Given the covariance matrix  $G$ , we compute the eigenvalues and eigenvectors of the squared matrix  $G^T G$ . Since  $G^T G$  has dimension  $(m \times m)$  (where  $m$  is the length of  $\mathbf{x}$ ), we obtain as many eigenvalues as the number of  $\boldsymbol{\theta}$  and  $\boldsymbol{\rho}_{\text{DM}}$  parameters. The bigger the eigenvalue, the higher the covariance information encoded in the correspondent eigenvector. In particular, the ‘‘percentage of covariance information’’ contained in a subset of these eigenvectors is estimated as the percentage ratio between the sum of the correspondent subset of eigenvalues and the sum of all eigenvalues. Often, most of the covariance information ( $> 99\%$ ) is encoded in very few eigenvectors. We set a threshold at 99% and select the lowest number of eigenvalues (and eigenvectors) for which 99% is represented. Defining  $\mathbf{w}$  the matrix whose columns correspond to the selected eigenvectors,  $\mathbf{x}'$  is defined as

$$\mathbf{x}' \equiv \mathbf{w}^T \mathbf{x}. \quad (\text{C8})$$

Note that, by construction, the dimension of  $\mathbf{x}'$  is smaller than the dimension of  $\mathbf{x}$ .

<sup>3</sup> In Sec. II C we were able to compute  $\hat{\mathbf{a}}_0$  and  $\Sigma_0$  directly from the samples of the  $\boldsymbol{\theta}$  parameters (Eq. 19 and 20), without drawing samples of the Fourier coefficients  $\mathbf{a}$ . In this case, we are interested in the covariance between  $\mathbf{a}$  and  $\mathbf{x}$ , which cannot be estimated analytically from the  $\boldsymbol{\theta}$  parameters samples only.

We can now define the transformation matrix  $T_w$  as:

$$T_w \equiv \begin{bmatrix} Id_{n_{\text{aRN}}} & 0 \\ 0 & \mathbf{w}^T \end{bmatrix}, \quad (\text{C9})$$

where  $Id_{n_{\text{aRN}}}$  is an identity matrix of dimension equal to the number of Fourier components used to describe RN. Given

$$\Sigma_x \equiv \begin{bmatrix} \langle \mathbf{a}_{\text{RN}} \mathbf{a}_{\text{RN}}^T \rangle & \langle \mathbf{a}_{\text{RN}} \mathbf{x}'^T \rangle \\ \langle \mathbf{x}' \mathbf{a}_{\text{RN}}^T \rangle & \langle \mathbf{x}' \mathbf{x}'^T \rangle \end{bmatrix} = \begin{bmatrix} \langle \mathbf{a}_{\text{RN}} \mathbf{a}_{\text{RN}}^T \rangle & G \\ G^T & \langle \mathbf{x}' \mathbf{x}'^T \rangle \end{bmatrix}, \quad (\text{C10})$$

we can use the transformation defined in Eq. C9 to compute the mean  $\hat{\mathbf{a}}'_0$  and variance  $\Sigma'_0$ :

$$\begin{aligned} \hat{\mathbf{a}}'_0 &\equiv \begin{bmatrix} \hat{\mathbf{a}}_0 \\ \mathbf{x}' \end{bmatrix} \\ \Sigma'_0 &\equiv T_w \Sigma_x T_w^T. \end{aligned} \quad (\text{C11})$$

From Eq. C11, the distribution  $\mathcal{N}(\mathbf{a}_{\text{RN}}|\mathbf{x}', \boldsymbol{\rho}_{\text{RN}_0})$  is fully determined. (Possible numerical resolution issues related to reconstructing the normal distribution from Fourier coefficients samples are discussed in Appendix A.) Thus, we have all the elements to use Eq. C5 and move to *Step 2* to sample over the RN hyperparameters.

Note that, for completeness, here we also included the white noise hyperparameters in the PCA. This is not necessary, since white noise (and other deterministic signals) are not covariant with the GWB. In fact, in the method described in Sec. II C it is not needed to add  $\mathbf{x}'$  terms when deriving the normal distribution  $\mathcal{N}(\mathbf{a}|\mathbf{x}, \boldsymbol{\rho}_0)$ .

## 2. Results

We present now the results obtained with the method presented in Sec. C1 in the case of SPNA for the pulsars J1909-3744 and J1738+0333 (EPTA DR2new data [49]). In both cases, we first carried out an inference run over the white noise and DM variation hyperparameters (*Step 1*) considering EFACs and EQUADs specific for each observing backend, and DM variations as a Gaussian process with a flat-tail power-law spectrum. The RN was also included in the model as a Gaussian process with a flat-tail power-law spectrum, but with the corresponding hyperparameters fixed to  $\log_{10} A_{\text{RN}} = -12$ ,  $\gamma_{\text{RN}} = 5$  and  $\log_{10} k_{\text{RN}} = -5$ . Then, we carried out an inference run over the RN hyperparameters (*Step 2*) using the regularized likelihood (Eq. 18), with  $\hat{\mathbf{a}}'_0$  and  $\Sigma'_0$  are derived as discussed in Sec. C1 (Eq. C11). The resulting posteriors (green curves) are compared with the posteriors obtained with the time-domain likelihood (Eq. 11) for a full SPNA (blue curves).

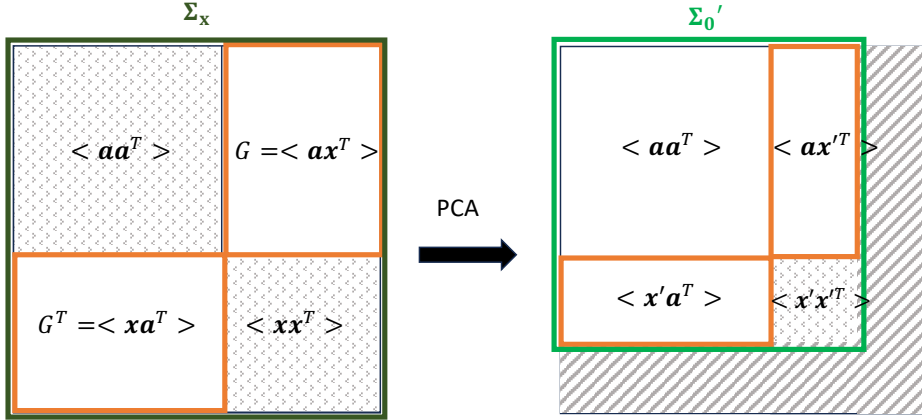


Figure 3. Visualization of the PCA approach. The squares are schematic representations of the covariance matrices of  $\Sigma_x$  (original set of variables, Eq. C10) and  $\Sigma'_0$  (after PCA, Eq. C11).  $\mathbf{a}_{RN}$  ( $\mathbf{a}_{RN} = \mathbf{a}$  in this visualization) are the Fourier coefficients that describe the achromatic noise processes included in the model.  $\mathbf{x}$  is the set of parameters investigated in *Step 1* (Eq. C6).  $\mathbf{x}'$  are optimized linear combinations of the parameters  $\mathbf{x}$  (Eq. C8). The parts of the matrices with the orange border contain the same covariance information. Note that  $\langle \mathbf{a}\mathbf{a}^T \rangle$  can be computed analytically:  $\langle \mathbf{a}\mathbf{a}^T \rangle = (F^T \hat{N}^{-1} F + \phi^{-1})^{-1}$  (See Eq. 19).

The posteriors for pulsar J1909-3744 are shown in Fig. 4. In this case, we can see that the correspondence between the blue (full SPNA with the time-domain likelihood) and green (Fourier-domain analysis with PCA approach to include the covariance between DM variations and RN hyperparameters) curves is perfect. This means that the result from the PCA on the Fourier coefficients  $\mathbf{a}_{RN}$  and the DM hyperparameters  $\boldsymbol{\rho}_{DM}$  well captures all the covariance between them, allowing us to marginalize over the DM hyperparameters and still obtain posteriors for the RN hyperparameters that are coincident to the posteriors for the RN hyperparameters obtained when  $\boldsymbol{\rho}_{DM}$  are also free parameters.

The posteriors for pulsar J1738+0333 are instead shown in Fig. 5. In this case, the obtained blue (full SPNA with the time-domain likelihood) and green (Fourier-domain analysis with PCA approach to include the covariance between DM variations and RN hyperparameters) posteriors are still compatible, but the green posteriors are narrower than the blue posteriors, showing a loss of information about the RN hyperparameters. We expect the two sets of posteriors to be identi-

cal, as it happens in the case of Fig. 4. The disagreement between the results in Fig. 5 implies that our method fails in including some of the covariance between RN and DM hyperparameters. Our best guess is that this is due to the little frequency coverage of pulsar J1738+0333 data, which does not provide enough information to successfully disentangle the two processes. In fact, from the posteriors shown in Fig. 1, one can see that the results for  $\boldsymbol{\rho}_{DM}$  and  $\boldsymbol{\rho}_{RN}$  are very similar. Furthermore, the EPTA noise analysis for this pulsar [50] also favored a model with only DM variations, unable to fully disentangle chromatic and achromatic red processes.

Thus, the method described in this section is suitable for pulsars (like J1909-3744) whose data have a wide frequency coverage and the noise analysis successfully disentangles chromatic and achromatic red signals. For the other pulsars, our method gives posterior distributions for the RN hyperparameters consistent with the posterior distributions obtained from the usual SPNA, but not equivalent.

The codes used to obtain the results in Fig. 4 and 5 are available at [52].

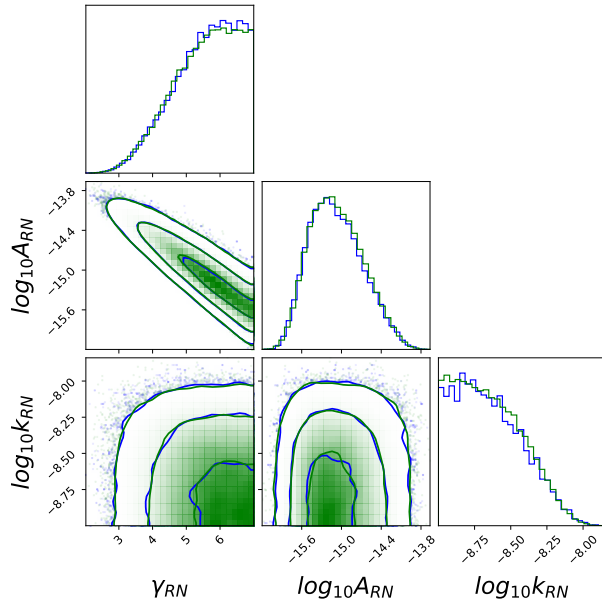


Figure 4. Posteriors for J1909-3744 RN hyperparameters obtained with the PCA approach (green curves) described in Sec. C1. The blue posteriors are instead the result of a full SPNA with the time-domain likelihood.

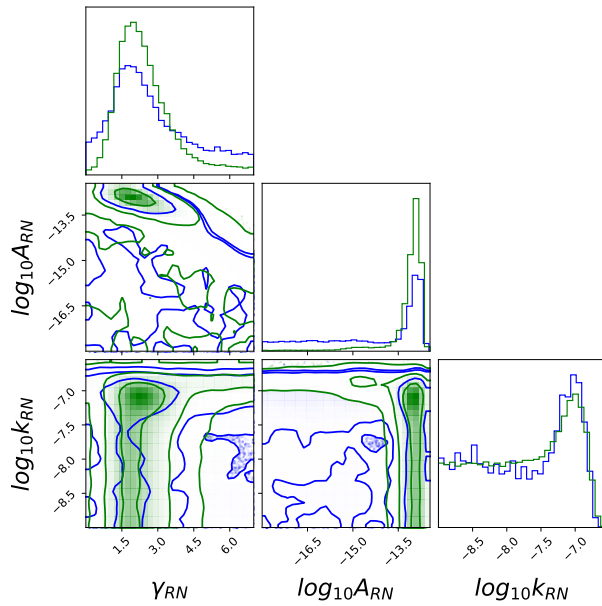


Figure 5. Posteriors for J1738+0333 RN hyperparameters obtained with the PCA approach (green curves) described in Sec. C1. The blue posteriors are instead the result of a full SPNA with the time-domain likelihood.